Functionalization of additive-manufactured Ti6Al4V scaffolds with poly(allylamine hydrochloride)/poly(styrene sulfonate) bilayer microcapsule system containing dexamethasone

Ekaterina Chudinova[1], Andrey Koptyug[2], Yulia Mukhortova[1], Artyom Pryadko[1], Anastasiya Volkova[1], Alexey Ivanov[1], Evgenii Plotnikov[1], Yelena Khan[1], Matthias Epple[3], Viktoriya Sokolova[3], Oleg Prymak[3], Timothy Douglas[4,5], Roman Surmenev[1], Maria Surmeneva[1,*]

[1]Physical Materials Science and Composite Materials Centre, Research School of Chemistry & Applied Biomedical Sciences, National Research Tomsk Polytechnic University, 30 Lenin Avenue, Tomsk 634050, Russian Federation

[2]Department of Mechanical Engineering and Quality Technology, SportsTech Research Centre, Mid Sweden University, Akademigatan 1, SE 831 25, Östersund, Sweden

[3]Inorganic Chemistry and Center for Nanointegration Duisburg-Essen (CeNIDE), University of Duisburg-Essen, Essen 45117, Germany

[4]Engineering Department, Lancaster University, Lancaster, United Kingdom

[5]Materials Science Institute (MSI), Lancaster University, Lancaster, United Kingdom

[*]corresponding author: surmenevamaria@mail.ru

Abstract

Porous titanium alloy Ti6Al4V scaffolds manufactured via electron beam melting (EBM®) reveal broad prospects for applications in bone tissue engineering. However, local inflammation and even implant failure may occur while placing an implant into the body. Thus, the application of drug carriers to the surface of a metallic implant can provide treatment at the inflammation site. In this study, we propose to use polyelectrolyte (PE) microcapsules formed by layer-by-layer (LbL) synthesis loaded with both porous calcium carbonate ($CaCO_3$) microparticles and the anti-inflammatory drug dexamethasone (DEX) to functionalize implant surfaces and achieve controlled drug release. Scanning electron microscopy indicated that the $CaCO_3$ microparticles

coated with PE bilayers loaded with DEX had a spherical shape with a diameter of 2.3±0.2 μm and that the entire scaffold surface was evenly coated with the microcapsules. UV spectroscopy showed that LbL synthesis allows the manufacturing of microcapsules with 40 % DEX. According to high performance liquid chromatography (HPLC) analysis, 80 % of the drug was released within 24 h from the capsules consisting of three bilayers of polystyrene sulfonate (PSS) and poly(allylamine)hydrochloride (PAH). The prepared scaffolds functionalized with $CaCO_3$ microparticles loaded with DEX and coated with PE bilayers showed hydrophilic surface properties with a water contact angle below 5°. Mouse embryonic fibroblast cells were seeded on Ti6Al4V scaffolds with and without LbL surface modification. The surface modification with LbL PE microcapsules with $CaCO_3$ core affected cell morphology *in vitro*. The results confirmed that DEX had no toxic effect and did not prevent cell adhesion and spreading, thus no cytotoxic effect was observed, which will be further studied *in vivo*.

Keywords: additive manufacturing, Ti6Al4V scaffolds, surface modification, calcium carbonate, microparticles, dexamethasone

1. Introduction

Currently, an increased number of people suffer from age-related diseases, such as osteoarthritis. Statistics show that more than 90 % of the population over the age of 40 have problems associated with the skeletal system dysfunctions and are at risk of orthopedic surgeries [1].

Titanium and its alloys are currently the most commonly used materials for endosseous dental implants and endoprostheses. Recent studies have demonstrated that titanium implants have a reliable success rate due to their good biocompatibility, corrosion resistance and relatively low elastic modulus [2, 3].

Although titanium meets the requirements as a material for a prospective orthopedic implant, currently used titanium implants reveal long-term failure rates due to infections, poor osseointe-

gration of the implants, which may result in inflammation. When a synthetic implant is inserted into the body, some specific immune system responses may be initiated, which result in a tissue encapsulation causing wear and abrasion. As a result of slowly developing problems, titanium implants reveal an average service lifetime of approximately 10-15 years before replacement is needed [2, 4].

In addition, the loosening of an implant can be caused by the metallic or polymeric wear debris, resulting in osteolysis and need for revision surgery. In further, wear particles at the tissue-implant interface can trigger the invasion of inflammatory cells (e.g., polymorphonuclear leukocytes, macrophages, monocytes, lymphocytes) and eventually fibroblasts, which causes acute and chronic inflammation and fibrosis [5].

A variety of pharmaceuticals (e.g. glucocorticoid) have also been used to overcome these challenges. As an example, the synthetic glucocorticoid dexamethasone (DEX) is used in clinics for the treatment of inflammatory bowel diseases, rheumatoid arthritis, posttransplantation immunotherapy and others [6]. DEX allows suppressing the immune response by reducing lymphatic activity, it also stimulates osteogenic differentiation and promotes metabolism of protein, fat and carbohydrate [7]. In addition, the stimulation of osteogenic differentiation is advantageous for materials to promote bone formation.

Implant-associated inflammation following invasive orthopedic surgery is one of the major clinical problems that can cause implant failure [8]. Advances in nanotechnology have led to the development of novel implant materials that not only have better cytocompatibility, but can also be used as multifunctional drug delivery platforms [9].

Among the different inorganic drug carriers, calcium carbonate ($CaCO_3$) nano- and microparticles show unique advantages due to their ideal biocompatibility and potential for use as a controlled delivery system for loading different types of drugs. The accessibility, low cost, safety, biocompatibility, pH-sensitive properties, osteoconductivity and slow biodegradability of $CaCO_3$ particles make them suitable drug delivery carriers. Due to a slow degradation rate of $CaCO_3$,

$CaCO_3$-based particles can be used as sustained release systems that retain their cargo for long times after administration. Such particles with good osteoconductivity and bioresorbability are a proper dual-mode solution for bone substitution and drug release in bone-related diseases, such as osteomyelitis. Different types of particulate $CaCO_3$ have also shown notable applications in filling bone defects, treating early dental caries lesions and generating newly formed bone tissue. According to the reviewed literature, $CaCO_3$ nano- and microparticles show potential both as bone substitutes and drug carriers in bone-related disease/defects because of their special characteristics [10, 11].

We have already presented a study on the application of $CaCO_3$ as a potential drug carrier [12]. Based on the presented literature review and the studies already carried out, the main goal of this particular work is to modify the surface of additive manufactured Ti6Al4V scaffolds by using particles with porous $CaCO_3$ cores loaded with DEX, providing controlled drug release, and coating with PE bilayers with the aim to show the possibility of achieving a multiple effect of both improved surface bioactivity due to calcium carbonate and anti-inflammatory properties via the release of encapsulated dexamethasone. The presented method of surface functionalization of the scaffolds is presented for the first time.

2 Materials and methods

2.1 Fabrication of titanium alloy scaffolds

This study was based on porous titanium alloy Ti6Al4V scaffolds manufactured by powder bed additive manufacturing via electron beam melting (EBM®) using an ARCAM A2 EBM® machine (Arcam EBM, Sweden). The process used a standard precursor powder supplied by Arcam EBM with a grain size distribution between 50 and 125 µm and a layer thickness of 70 µm and machine-default process parameter settings. The process was carried out at a pressure of 10^{-4} Pa while keeping the working area temperature at 730 °C. The process is described in detail elsewhere [13].

2.2 Synthesis of calcium carbonate microparticles

The cores of $CaCO_3$ were obtained by mixing a solution of $CaCl_2$ (1 M), DEX (4 mg/ml), and Na_2CO_3 (1 M) with a magnetic stirrer at a rate of 1100 rpm for 25 min. The suspension of particles was precipitated by centrifugation at a rate of 9000 rpm for 3 min, followed by the removal of supernatant. Then, the cores were washed with deionized water, ultrasonicated, and again precipitated by centrifugation under the same conditions. The washing process was repeated 2 times. After the second washing step, 10 µl of the suspension with particles was taken for zeta potential and particle size measurements.

2.3 Polyelectrolyte bilayer assembly

Two oppositely charged PEs, namely, polystyrene sulfonate (PSS, a negatively charged polymer) and poly(allylamine)hydrochloride (PAH, a positively charged polymer), were used as layers for $CaCO_3$ cores loaded with DEX. The bilayer assembly was prepared by adsorption of PEs (2 mg/ml, both in 0.15 M NaCl). The first single layer PAH was allowed to adsorb onto $CaCO_3$ particles loaded with DEX for 10 min. After that, the suspension was centrifuged at 1300 rpm for 3 min and washed three times with deionized water to remove the non-adsorbed polyelectrolyte. In addition, gentle shaking followed by 3 min of ultrasonication was used to avoid particles agglomeration after centrifugation. Next, the deposition of PSS was carried out on the PAH-coated $CaCO_3$ particles with loaded DEX using the same manipulation.

2.4 Deposition of particles on titanium alloy scaffolds

The porous Ti6Al4V scaffolds were immersed in a 2 ml water-based solution with 40, 200 and 400 µl aliquots containing particles to achieve final concentrations per 1 ml of $5.3 \cdot 10^5$ and placed into a shaker for 90 minutes at room temperature. Then, the scaffolds were dried at room temperature. A schematic overview of this process is shown in Figure 1.

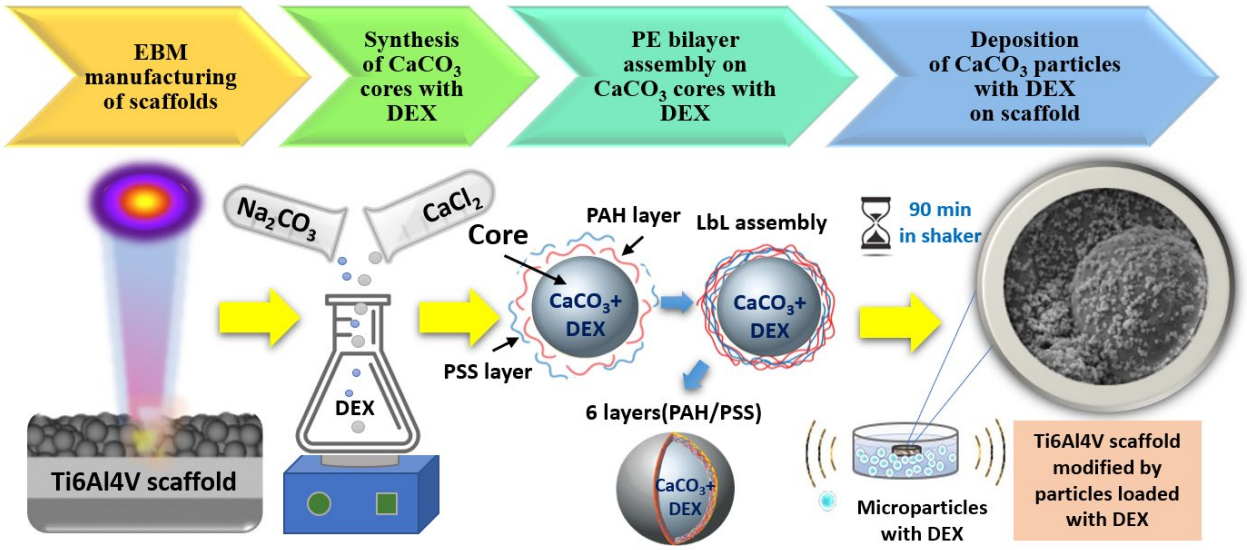

Figure 1 Schematic illustration of the process of Ti6Al4V scaffold modification via $CaCO_3$ microparticles loaded with DEX and coated with $(PAH/PSS)_3$.

2.5 Scanning electron microscopy and elemental composition

Scanning electron microscopy (SEM) imaging of $CaCO_3$ microparticles loaded with DEX and coated with PE bilayers was performed using a Quanta 200 3D microscope (FEI, USA). The tests were carried out on microparticles with remaining and dissolved $CaCO_3$ cores and scaffolds before and after functionalization by microparticles and modified scaffolds after the test with fibroblasts. The operating voltage was 20 kV. For the SEM studies, one droplet of the sample suspension with particles was applied onto a silicon wafer and dried for 2 hours at 37 °C. To assess the wall thickness via SEM, the core was removed from the capsules using ethylene diamine tetraacetic acid (0.2 M, pH 6). Then, the capsules were washed 2 times with distilled water by centrifugation at 3500 rpm for 7 min. Scaffolds after dip-coating were dried overnight under ambient conditions. An energy dispersive spectroscopy (EDS) analysis was performed using the SEM-EDX-EMAX analysis tool to identify the chemical composition of the samples.

2.6 Particle size and zeta potential

The hydrodynamic diameter (HDD) of the microparticles was measured using a Malvern Zetasizer Nano ZS system (Malvern Instrument, UK) based on dynamic light scattering (DLS). Size measurements were performed in triplicate. For these measurements, 10 µl of the suspension with microparticles was diluted 100 times with deionized water at room temperature. Zeta potential was measured using the same instrument and conditions. The polydispersity index range was between 0 and 1.

2.7 Encapsulation efficiency of DEX

The suspensions of the DEX-loaded $CaCO_3$ cores in deionized water were centrifuged at 9 000 rpm for 3 min, and the loading efficiency of the loaded DEX was determined by quantifying the absorption of the clear supernatant using ultraviolet and visible (UV-Vis) spectroscopy (Cary 300 Bio UV-Vis-spectrophotometer, Varian). The corresponding calibration curves were made by testing pure DEX and supernatant solution after the primary collection of microparticles. The absorbance values of DEX and PSS were measured using a UV–Vis spectrophotometer at wavelengths of 242 and 226 nm, respectively. Tests were performed four times for each sample. The encapsulation efficiency of DEX in the $CaCO_3$ core is determined using the following equation [14]:

$$EE\% = \frac{W_l}{W_t} \cdot 100\%,$$

where W_t is the total amount of loaded substance and W_l is the amount of free substance in the supernatant after centrifugation.

2.8. Infrared (IR) spectroscopy

The molecular bonds of the $CaCO_3$ microparticles without and with DEX were analyzed by IR spectroscopy (Vertex 70, Bruker). For these tests, the capsules were dried in an oven at 55 ℃ for 12 hours. Using a hydraulic system, a pellet was prepared from a mixture containing 2 mg of

dried particles with and without DEX and 200 mg of powdered KBr. Spectral analysis was performed in transmission mode over the range 4000–500 cm^{-1} with a spectral resolution of 2 cm^{-1}.

2.9 Contact angle and surface free energy

Wettability measurements of the surface were carried out using an Easy Drop DSA1 system (Kruss, Germany). The contact angles (CAs) of three reference liquids were measured with the sessile drop method. The wettability studies were performed with a video contact angle system. The measurements were obtained at room temperature (22 °C). At least five measurements with a droplet volume of 3.5 µL were carried out with three different samples in each series. To determine the surface free energy of the modified surfaces, the contact angles were measured with the liquids water (polar), ethylene glycol (polar) and glycerol (non-polar). The values of the surface tension of water, ethylene glycol and glycerol are 72.1, 47.4 and 63.4 mN/m, respectively. The calculations of the surface free energy of the functionalized scaffolds were performed using the Owens-Wendt equation (1):

$$\frac{\sigma_L(\cos\theta+1)}{2\sqrt{\sigma_L^D}} = \frac{\sqrt{\sigma_S^P}\cdot\sqrt{\sigma_L^P}}{\sqrt{\sigma_L^D}} + \sigma_S^D \quad (1)$$

where σ_L^D, σ_S^D, σ_L^P, and σ_S^P are the dispersive and polar components of the surface free energy of the liquid (L) and solid (S) phases, respectively, whereas σ_L is the surface free energy of the test liquid.

2.10 Roughness measurements

A Hommel Tester T100 (Germany) instrument was used to assess sample surface roughness. Four specimens of each scaffold (blank Ti6Al4V and 40, 200 and 400 µL aliquots of $CaCO_3$ microparticles loaded with DEX) were selected randomly (five measurements per scaffold). The average roughness (R_a), maximum roughness (R_{max}) and peak-to-valley roughness (R_z) were measured.

2.11 *In vitro* release

2.11.1 Preparation of scaffolds

Scaffolds modified with microparticles loaded with a 400 µl DEX aliquot were dried for 48 hours at room temperature in a laminar flow box and loaded into sterile containers with covers. Then, 5 ml of phosphate-buffered saline (pH 7.4) was added to each container, and the covers were closed and carefully sealed with paraffin film (Parafilm). The release test was carried out in a sterilized drying cabinet under static conditions at a temperature of 37 °C. The samples were taken and analyzed after 1, 3 and 7 days. The solution from the containers was analyzed by high-performance liquid chromatography (HPLC) at λ_{max} = 242 nm to determine the content of released DEX. The concentration of DEX in the analyzed solutions was determined using a calibration curve.

2.11.2 High-performance liquid chromatography

High performance liquid chromatography (HPLC) was performed on an HPLC Agilent 1200 system with a diode array detector (1260 DAD VL). The spectrophotometric analysis was performed on an Evolution 600 UV-VIS spectrophotometer (Thermo Scientific Corp., USA), and samples were loaded in matched quartz cuvettes with a 1 cm path length. All aqueous solutions, including the HPLC mobile phase, were prepared using a Milli-Q IQ 7003 (Merck) water purification system. HPLC-grade acetonitrile was obtained from Panreac, and TFA and PSS were obtained from Sigma-Aldrich.

Chromatography was carried out using a Zorbax (Agilent Technologies, U.S.A.) Eclipse Plus C18 column (4.6 mm · 150 mm, 5 µm) at 30 °C. Analysis was performed using 0.1 % trifluoroacetic acid in H_2O (phase A)–CH_3CN (phase B) as the mobile phase, which was introduced by gradient elution from 0 to 50 % phase B for 10 min at a flow rate of 1 ml/min. After the end of analysis, the elution condition was set to introduce the initial phase (100 % A) for 10 min. The

injection volume was 20 µL. UV detection was carried out at characteristic wavelengths of 242 nm for DEX and 230 nm for PSS. The retention times were 9.0 min for DEX and 5.4 min for PSS. The method was partially validated with respect to its calibration curve (regression equation: y=32986x-8.22; R^2=0.9998; over a concentration range of 1.2-20 µg·ml^{-1}), precision of the area (RSD value ranging between 0.1 and 1%), accuracy (between 98 and 102 % at the different concentrations), LOD=0.03 µg/ml and LOQ=0.1 µg/ml (calculated by the signal-to-noise ratio (S/N); for the LOD, S/N=3, and for the LOQ, S/N=10). Before analysis, every sample was filtered through a 0.45 µm nylon syringe filter. Each sample was analyzed three times.

2.12 Cell culture tests

The mouse embryonic fibroblast line 3T3-L1 (ATCC CL-173) was used for all cell experiments. Cells were cultured in complete DMEM (Gibco, USA) supplemented with glutamine (GlutaMAX, Gibco, USA), 10 % fetal bovine serum (One Shot™, TFS, Brazil) and antibiotics (a penicillin/streptomycin mixture, Paneko, Russia). Fibroblasts were maintained in a CO_2 incubator (5 % CO_2) at 37 °C with saturated humidity. When the cells reached 70 % confluence, they were detached by trypsin (0.05 % trypsin-EDTA solution, Paneko, Russia) and used in tests. Prior to the cell tests, titanium scaffolds with and without surface modification were pretreated for 10 min in ethanol solution, washed for 5 min in phosphate buffer and transferred to a 6-well plate. Next, 3.0 ml of the fibroblast suspension ($50 \cdot 10^3$ cells/ml) was added to each well (equivalent of $150 \cdot 10^3$ cells per well), completely covering the scaffold surface. After that, all the samples were placed in a 37 °C incubator for 24 hours.

2.13 Cell proliferation and morphology assessment

The attachment, morphology, proliferation and growth density of cells were assessed by fluorescence microscopy after 24 hours of incubation. The culture media was removed, and the vital fluorescent dyes calcein AM (0.5 µg/ml) and Hoechst 33342 (1 µg/ml) in phosphate buffer were

added to cover the surface of the scaffolds with living cells. This allows for detection of the nucleus and cytoplasm and for easy differentiation of living cells. Plates with fluorescent dyes were kept for 15 minutes in an incubator at 37 °C. Then, the scaffolds were gently washed in phosphate buffer, and microscopic examination was carried out using a microscope (Zeiss Axiovert A1) with appropriate light filters. Micrographs were taken in different fields of view in three repetitions. Image processing was performed by ZEN Pro software (Zeiss). Cell density was calculated with ImageJ software.

3 Results and discussion

3.1 Characterization of $CaCO_3$ microparticles loaded with DEX

Figure 2 displays micrographs of $CaCO_3$ microparticles before (a) and after dissolution of cores (b) prepared with the LbL procedure. Characterization results confirm the presence of spherical $CaCO_3$ microparticles with a uniform size distribution from 2 to 3 μm (Fig. 2a,c). Images reveal that the surface of the scaffolds is well-developed and coated with many calcium carbonate microparticles. Studies also show that despite the difference in size, hybrid particles have similar morphologies. Note that after dissolution of the cores, the resulting microparticles become asymmetric (Fig. 2b).

In our case, carbonate cores, removed from the shell by a chelating agent, were also left in the assembly [15]. This decision was dictated by several reasons. First, $CaCO_3$ microparticles made it possible to fix a larger amount of low molecular weight drug in polymer capsules (reducing drug losses during the synthesis of capsules), which was required to provide a therapeutic effect. Second, $CaCO_3$ is a supplier of the calcium ions necessary for the formation of new bone. Thus, the diameter of the particles with the cores after drying is approximately 2 μm, and the wall thickness of the particles with the dissolved core is 360 nm (Fig. 2d). Note that the particle size depends on the reagent concentration and stirring rate, and the size decreases with their decrease [16, 17].

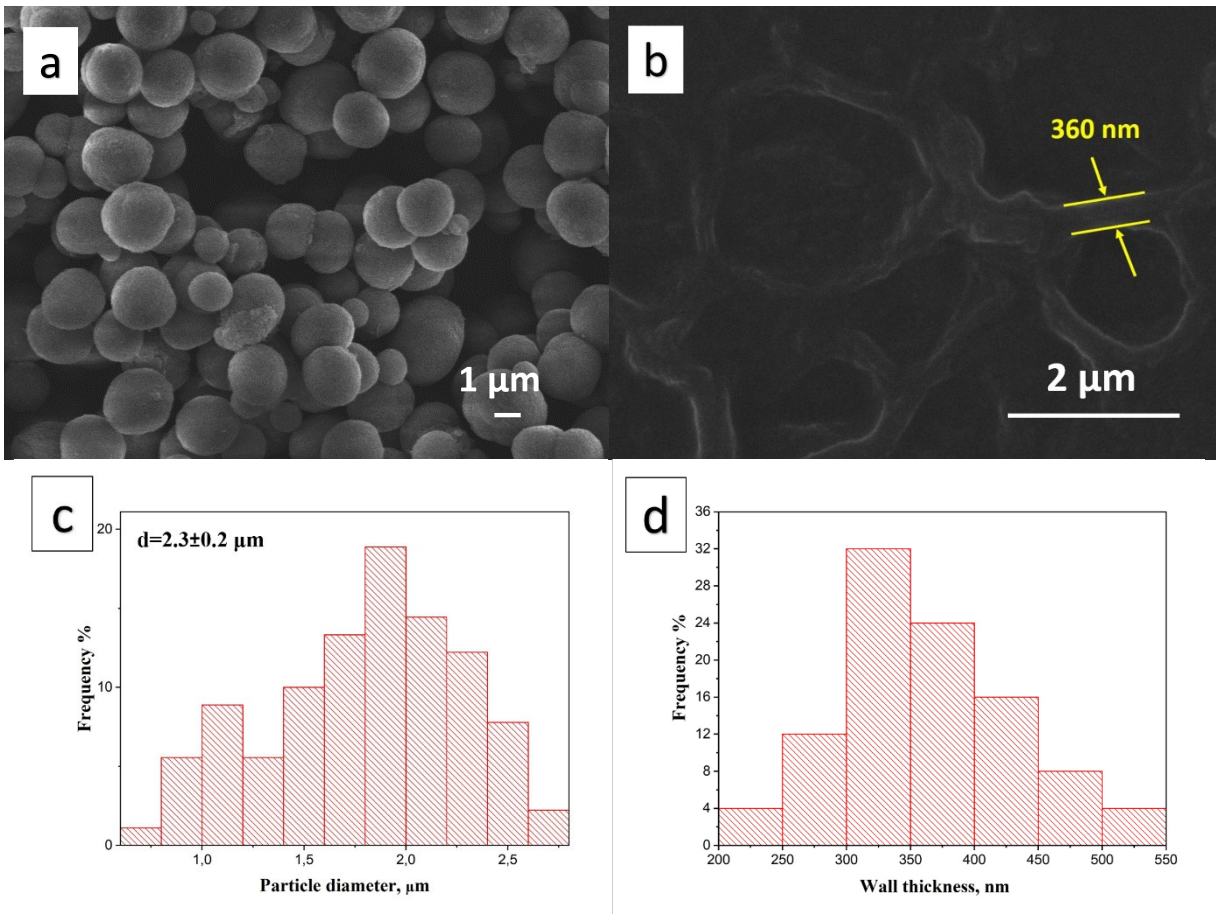

Figure 2 SEM image of microsphere-loaded DEX prepared by LbL synthesis before (a) and after dissolution of cores (b); histograms indicating the particle size (c) and wall thickness (d) distribution.

Figure 3 presents the DLS measurement results obtained for the microparticles. The layer-by-layer assembly of PAH/PSS on the $CaCO_3$ cores can be observed from the changes in the zeta potential after the deposition of each PE layer. Figure 3 shows the reversal of the surface charge with the deposition of PE layers. The bare $CaCO_3$ cores were negatively charged, and their zeta potential was -17.6±1.6 mV. The absorbed PAH layer changed the surface electrical charge to +10.3±1.1 mV, and the PSS layer reversed it to -17.7±1.6 mV. In addition, the coatings resulted in similar changes in the zeta potential. Alternation in the zeta-potential values indicated that the layer-by-layer assembly of PEs on the DEX-loaded $CaCO_3$ cores was successful. Similar changes in the zeta potential were observed and previously reported for different PEs producing oppositely charged layers on the $CaCO_3$ cores [18-21].

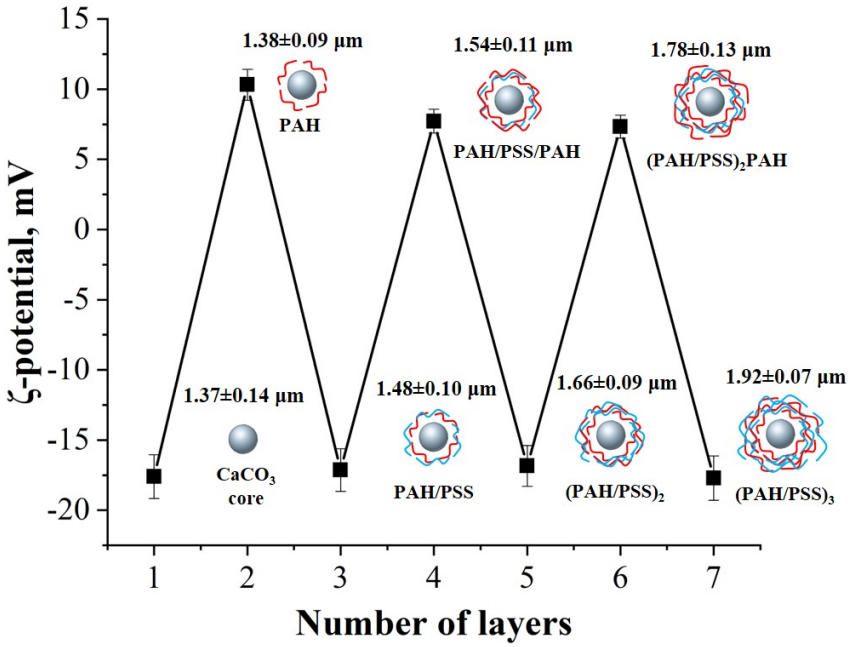

Figure 3 Zeta potential of PE microparticles loaded with DEX and coated with PE bilayers, as measured by DLS.

3.2 Loading efficiency and chemical composition

The loading efficiency clearly depends on the composite particle preparation procedure. Among the influencing factors are the ways in which active substances are encapsulated, the number of PE bilayers, the size and resulting porosity of the PE microparticles, etc. [22]. In our case, the LbL method of particle synthesis allowed loading up to 40 % DEX and 51 % PSS (calibration curves are presented in Figure 4a,b).

Previous reports [19] showed that DEX-loaded PE-coated alginate microspheres were fabricated by the droplet generator technique with a DEX encapsulation efficiency of 77 %. Seijo et al. [23] reported a DEX entrapment efficiency of 75 % in poly-(isobutylcyanoacrylate) (PIBCA) nanospheres prepared by the *in situ* polymerization procedure. Song et al. [24] reported a drug entrapment of 79.6 % in PLGA nanospheres obtained using the emulsification/solvent evaporation technique. In addition, Fessi et al. [25] achieved a drug entrapment of 40 % in capsules prepared by the nanodispersion of preformed poly(DL-lactide). Panyam J. et al. performed the direct ex-

traction of a drug from particles and attempted to determine the drug loading amount in particles; however, this method resulted in approximately 20 to 30 % recovery of the encapsulated drug [26].

In addition, Mandapalli and coworkers [27] investigated factors that may affect the encapsulation efficiency of $CaCO_3$ self-assembled LbL microparticles (LbL-MC), such as incubation time, solute concentration, pH and ionic strength, using ascorbic acid, imatinib mesylate and 5-fluorouracil as model molecules. They showed that the encapsulation efficiency of LbL-MC increased linearly with increasing solute concentration. The change in pH from 2 to 6 increased the encapsulation efficiency of the charged molecules in LbL-MC [27]. It was also shown that hybrid cyclodextrin-calcium carbonate porous microparticles loaded with coumarin and Nile red are more efficient for loading hydrophobic dyes than bare $CaCO_3$ microparticles [20]. IR spectra of the hollow and DEX-loaded microparticles coated with PE bilayers particles tested in the present research are shown in Figure 4c.

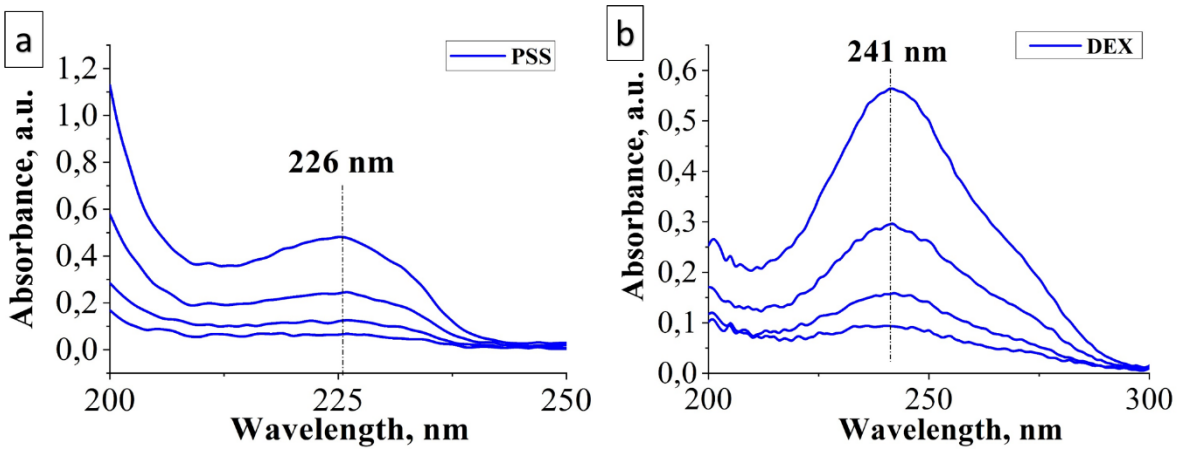

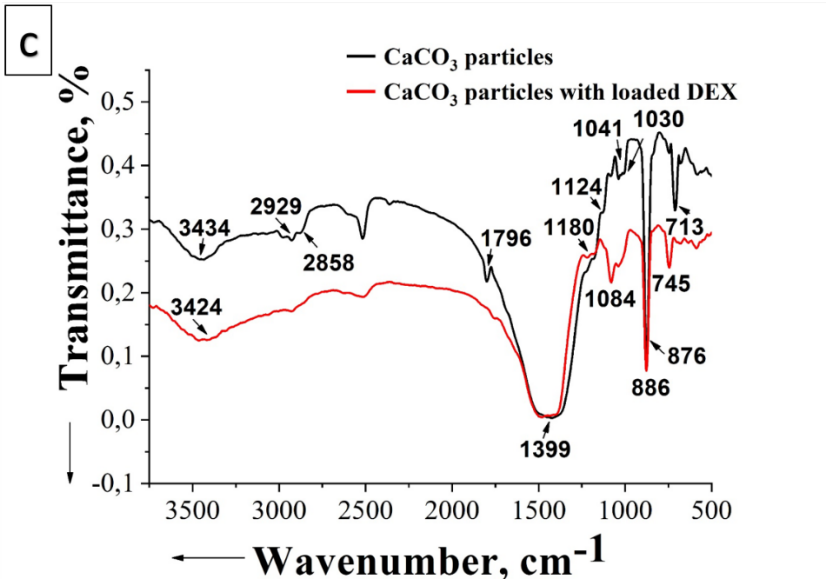

Figure 4 The absorbance spectra of the control $CaCO_3$ microparticles (a) and DEX-filled microparticles (b) recorded near the characteristic wavelength at different concentrations and their IR spectra (c).

The corresponding spectra of microparticles loaded with DEX show the characteristic absorption bands at 3424 cm^{-1}, 2929 cm^{-1} and 1084 cm^{-1} corresponding to the hydroxyl groups (-OH), CH_2 and C-O stretching vibrations, respectively. Additionally, the absorption band at 1399 cm^{-1} ascribed to the C-F stretching vibration of DEX [28] is also clearly observed (Fig. 4c). The stretching band of phosphate anions (P-O) appears at 1041 cm^{-1} for the tested DEX-loaded microparticles, indicating successful intercalation of dexamethasone phosphate [29]. The characteristic C-O stretching band of vaterite can be observed at 745 cm^{-1} [30]. The presence of the calcite phase is confirmed by the characteristic bands at 876 and 713 cm^{-1}, which correspond to out-of-plane bending vibrations and doubly degenerate planar bending vibrations, respectively [31-33]. Characteristic carbon-nitrogen bond spectral features are observed at 800–920 cm^{-1}, signifying the presence of PAHs [34]. The features at 1030 and 1180 cm^{-1} are characteristic of the O–S–O and S=O bonds [35], confirming the presence of PSS. Additionally, two peaks corresponding to SO^{3-} stretching vibrations can be discerned at 1124 and 1160 cm^{-1} [36, 37]. These observations confirm the successful deposition of PSS and PAH on the $CaCO_3$ core.

3.3 Morphology and roughness after surface modification

There are multiple reports on the surface modification of Ti6Al4V samples by various coatings, including nanotubes and micro- and nanoparticles [38, 39]. In this study, we developed a new method of scaffold functionalization based on the deposition of PE-coated microparticles with a $CaCO_3$ core loaded with DEX targeting simultaneous supports for osseointegration and prolonged controlled drug delivery. The $(PAH/PSS)_3$ microspheres were synthesized through a self-assembly process, and the dip-coating method was used to prepare hybrid Ti6Al4V scaffolds with surface coatings by using $CaCO_3$ microparticles loaded with DEX and coated with PEs.

The details on the procedure to prepare the EBM® samples and macroscopic images of the surface topography of the samples can be found elsewhere [40]. The surface topography of the metallic scaffolds is highly dependent on the precursor powder size and size distribution, which is reported elsewhere [41, 42].

The SEM images (Fig. 5a-b, d-e, g-h) showed that the particles prepared with different DEX aliquot volumes of 40, 200 and 400 µl per 2 ml of suspension were successfully immobilized on the surface of Ti6Al4V scaffolds. In the case of the smallest concentrations of particles, they were deposited primarily in the valleys of the scaffold surfaces (Fig. 5a,b).

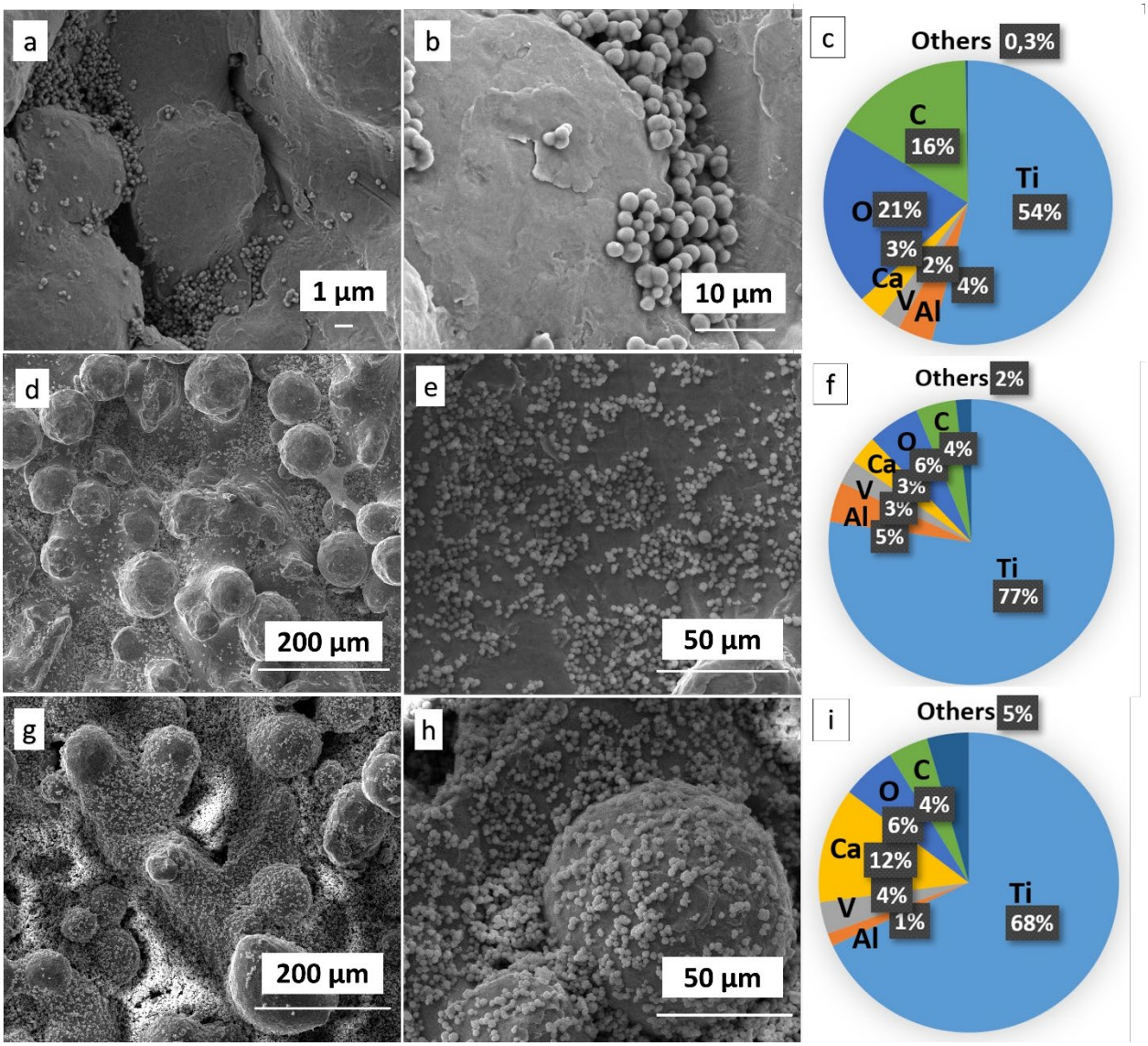

Figure 5 Scanning electron images of the Ti6Al4V scaffolds functionalized with microparticles loaded with DEX in different regimes with aliquot of 40 (a, b), 200 (d, e) and 400 (g, h) µL aliquots and the corresponding content of chemical elements in at.% obtained via EDS (c, f, i).

According to the calculations, for the scaffolds immersed in the suspension containing a 400 µl aliquot of synthesized microspheres per 2 ml of suspension, the corresponding average surface density of the microparticles was 0.05 mg·cm^{-2} or 7.1 · 10^6 particles per cm^2. Note that the number of microparticles on the surface will proportionally increase with an increase in the concentration of the suspension used. Thus, the number of particles per cm^2 deposited in suspension with 40 and 200 µl aliquots of DEX per 2 ml was 3.6 · 10^6 and 0.9 · 10^6, respectively.

Similar studies on drug loading were conducted by Timin et al. [15]. In their case, PCL, PHB and PHB-PANi polymer scaffolds were modified by degradable hybrid silica microparticles loaded with DEX used as a low-molecular weight osteoinductive factor. The DEX content in the scaffolds was calculated to be 0.07 $mg \cdot cm^{-2}$. Note that in the case of polymer scaffolds, their surface areas are quite large due to the fibrous structure, which facilitates the deposition of many microparticles. It is shown in this work that depending on the type of polymer, the surface morphology changes after modification. Karpov et al. tested the deposition of particles loaded with growth factors on polymer scaffolds [43].

Note that microparticles are mainly concentrated in the valleys of the scaffold surface (Fig. 5a,d,g), which can be explained by adhesive interactions and rheology. Interparticle adhesion is caused by intermolecular forces, including van der Waals forces, local chemical bonds, electrostatic charges, and bridging forces, namely, surface liquid capillary attractions. These forces are strongly affected by surface properties, such as texture, surface chemistry, adsorption layers, and contact area. For larger particles, their gravity and inertia in near-surface flow are generally greater than the interparticle adhesion force; hence, they normally flow easily. For fine particles (less than ~10 μm), the interparticle adhesion force is appreciable relative to gravity [44]. The distribution of the microparticles loaded with DEX on the titanium alloy scaffold is illustrated in Figure 6. Microparticles are mainly concentrated in the valleys and surface crevices. The powder grains that partially fused into the sample surface are almost uncoated when a low concentration of microparticles is used (Fig. 5a,b). With increasing microparticle concentration, coating the partially fused powder grains becomes increasingly more effective (Fig. 5d, e and g, h).

Figure 5c, f, i demonstrates the atomic percentages of the chemical elements of the modified scaffolds, as measured by EDS. Calcium, oxygen and carbon were the main elements detected in the coating, which confirmed the successful immobilization of microparticles on the surface of the scaffolds.

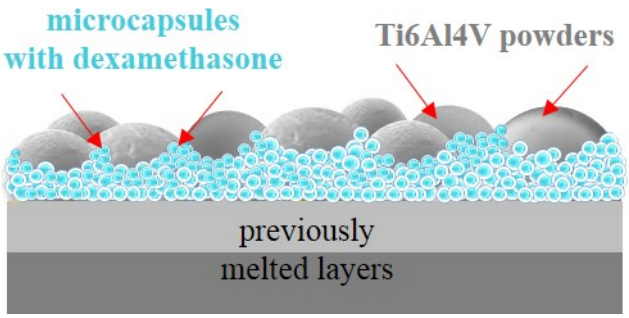

Figure 6 The principle of the arrangement of microparticles loaded with DEX on the surface of additively manufactured Ti6Al4V scaffolds.

Note that the surface charge is an important parameter that affects microparticle deposition over the surface. Table 1 illustrates this effect for different substrates and functionalizing agents.

Table 1 – Chemical characteristics of surfaces and polymers [45].

Surface	Charge	Hydrophilicity
Ti	Negative	Medium
Ti6Al4V	Negative	Medium
Ti6Al4V (AM)	Negative	Low
TiO_2	Negative	Medium-high
PSS	Negative, from sulfonates	Medium-high
PAH	Positive	Low

Ti and Ti6Al4V show similar hydrophilicity, and their charges are also very similar [46, 47]. The surface charge of the titanium oxide layer is believed to be a significant factor contributing to determining cellular interactions. Upon contact with water, titanium oxide forms hydroxide groups on its surface, and owing to the amphoteric nature of titanium oxide, these groups can either become positively or negatively charged depending on the pH of the surrounding fluid. Thus, the passive oxide layer is negatively charged at physiological pH [48]. In our case, the medium was alkaline. In NaOH, this passive film dissolves, and an amorphous layer containing

positively charged alkali ions is formed on the surface [49]. Thus, the forces arising from the deposition of a negatively charged outer layer of microparticles with a PSS outer layer and a positively charged oxide layer can contribute to the adhesion of microparticles on the surface of the scaffolds.

Numerous theories explaining the influence of the thickness, structure, chemical composition and topography of the titanium oxide surface layer on its hemocompatibility have been proposed. The passive oxide film behavior on Ti alloys plays a crucial role in their suitability as implant materials. In addition, as reported elsewhere [48], Ti6Al4V without any additional chemical surface treatment is negatively charged at physiological pH. Native surface oxide overlayer formation and charging have been reported for e-beam additive manufactured nickel and titanium alloys [50]. Cordero et al. noted that the overlayer and native oxide that forms on bulk Ti6Al4V under ambient conditions have similar compositions, and the alloy particle overlayer is significantly thicker. In light of the results obtained and those of other studies on the surface chemistry of atomized powders, it appears that atomized powders have a thick oxide scale, which can electrically insulate the particles and cause their charging during e-beam additive manufacturing [50].

As shown by Tong et al. [51] the charge of the surfaces, particularly polymer ones, has a significant effect on the control of the permeability of the microparticles. Thus, as a shell, negatively charged poly(sodium-4-styrene sulfonate) (PSS) is electrostatically bonded to the positively charged poly(allylamine hydrochloride) (PAH) chains via Coulomb interactions [52].

Figure 7 illustrates how surface functionalization by microparticles loaded with DEX changes the average surface roughness, R_a, peak-to-valley roughness, R_z and maximum roughness, R_{max}. Average R_a values of 23±2 μm, 20±1 μm, and 19±1 μm were found for the 40, 200, and 400 μl aliquots per 2 ml of particle suspension, respectively.

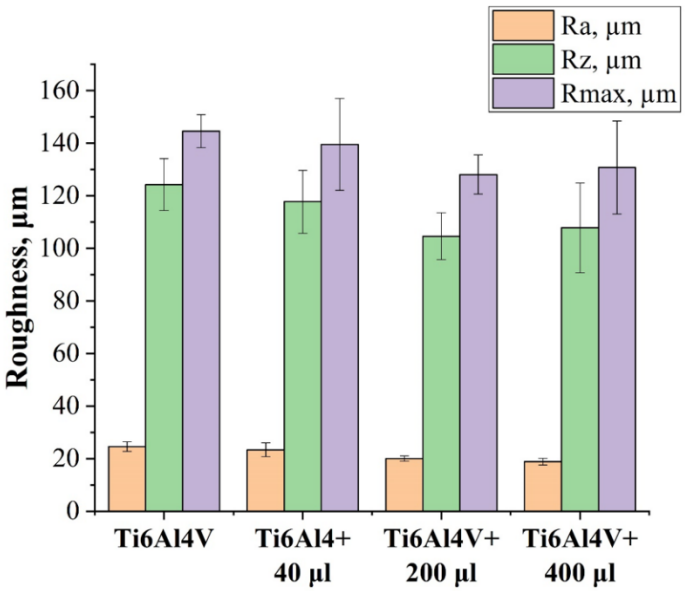

Figure 7 Roughness measurements of the Ti6Al4V scaffolds functionalized via microparticles loaded with DEX and coated with PE bilayers with 40, 200 and 400 µl aliquots per 2 ml.

Thus, R_a insignificantly decreases with increasing microparticle concentration. This can be explained by the fact that the microspheres located in the valleys of the scaffold fill the space between the melted titanium alloy particles and only slightly contribute to smoothing the surface, while the R_a value is still defined by larger features, including partially fused powder grains (Fig. 6). The maximum surface roughness value of R_a = 25±2 µm was obtained for the control scaffolds without functionalization. The R_z parameter reflects the local height fluctuations in a given area. Scaffolds treated with 40 µl aliquots of microparticles per 2 ml had R_z and R_{max} values of 118±12 µm and 132±3 µm, respectively, those treated with 200 µl aliquots per 2 ml had values of 109±5 µm and 127±4 µm, respectively, and those treated with 400 µl aliquots per 2 ml had values of 100±7 µm and 118±2 µm, respectively. This shows that the 400 µl sample has a smoother surface than scaffolds with a lower concentration of particles on their surfaces.

As noted in the literature, surface roughness influences van der Waals and capillary forces by affecting the contact area and capillary condensation between a particle and a surface [53]. As noted elsewhere [54], simulations indicate that both the capillary force and the van der Waals force (absolute value) increase as the particle size increases. When the particles are separated

from each other, the capillary and van der Waals forces gradually decrease with decreasing particle concentration. Thus, it can be concluded that the stronger the adhesive properties of the surface are, the higher the concentration of microparticles on this surface.

3.4 Wettability and surface free energy

A detailed study of the scaffold surface wettability was performed using the contact angle sessile drop method. The contact angle changes over 30 minutes for the scaffolds before and after deposition of the microparticles (Figure 8a). Note that the water contact angle revealed significant effect of surface modification of the scaffolds with microparticles.

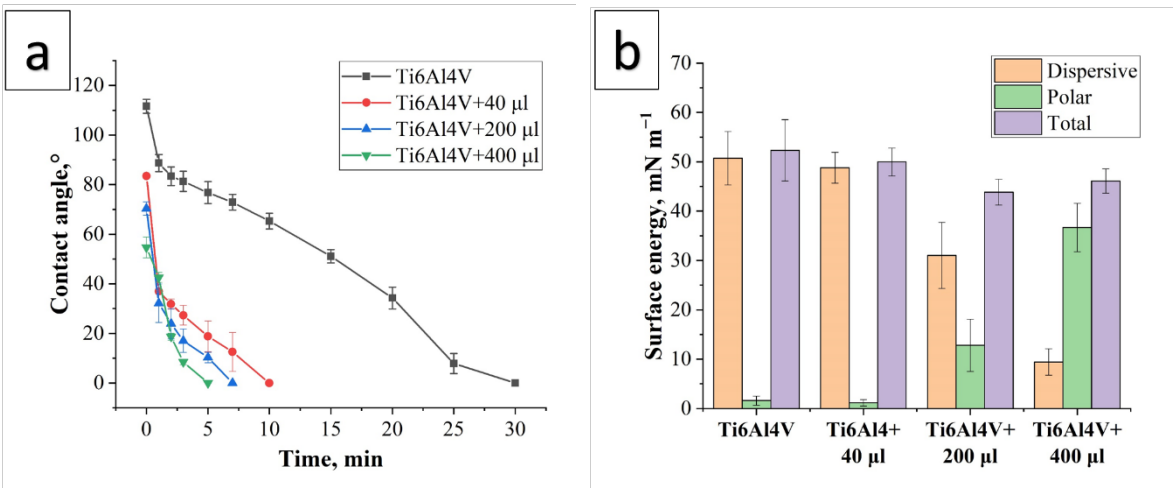

Figure 8 The results of the contact angle (a) and surface free energy (b) measurements of the Ti6Al4V scaffolds functionalized by 40, 200, and 400 µl aliquots of microparticles loaded with DEX per 2 ml.

The results showed a gradual decrease in the CA value over time during the first minutes of the experiment from the moment the water droplet was seeded on the surface. The droplet deposited on the functionalized surface of the Ti6Al4V scaffolds spread over the surface in 5, 7 and 10 minutes, showing CA values of less than 5° for the samples treated with 40, 200, and 400 µl aliquots of microparticles per 2 ml, respectively, which indicates the hydrophilicity of the surface. The control scaffold revealed the roughest surface and the most hydrophobic behavior, with a wetting angle of 112±3° in the first minutes and a spreading time of 30 minutes. This behavior

can be explained by the appearance of a passive oxide layer on the Ti6Al4V scaffold surface, which is known to be more hydrophilic due to the single bonded OH and single bonded O^{2-} groups formed on the outermost layer [55].

Wettability measurements showed a decrease in the contact angle with the increase in the concentration of PE-coated microparticles loaded with DEX. In our analysis, surface wettability, the influence of the substrate and the surface PE layers PAH/PSS were considered based on the studies by Kolasińska M [56]. It can be concluded that for the surface coatings using microparticles with six or more PE layers (i.e., from three PAH/PSS bilayers), wetting seems to become independent of the substrate, although the microparticles are not coated on the surface by the uniform layer without gaps. According to references based on surface modification, the PSS synthetic polymer has a moderate hydrophilicity [57], whereas negatively charged PAH demonstrates a higher contact angle [58]. However, Elzbieciak M and coauthors noted that multilayers with polycations as the top layer are more hydrophobic than those terminated with polyanions. This effect is most likely caused by the fact that the surface of water is negatively charged on the side of the bulk aqueous phase [59]. In further, the effect of the hydrophobicity of PAH is confirmed in studies by Wong et al. [60]. In addition, similar contact angles were observed for coatings prepared using a binary layer of PAH/PSS under similar conditions [59].

Few investigators have related the influence of surface roughness on its wetting behavior. It was noted that the hydrophobicity of a surface with a water contact angle of more than 90° may be a result of significant underlying roughness [61]. Additionally, a very rough surface facilitates the formation of air pockets, changing some of the interfaces from liquid-solid to liquid-gas, impacting the intermolecular interactions and increasing the contact angle.

Additionally, the authors of the study [62] noted that the contact angle decreases with an increasing number of PE layers on the sample. Figure 8b shows the variation in the dispersive, polar and total surface free energy (SFE) of the as-manufactured and modified surfaces of scaffolds. The presented results show a slight decrease in energy with increasing particle concentration.

The highest SFE of the analyzed samples was obtained for non-modified scaffolds (52.32 ± 6.23 mN/m). In general, an insignificant decrease in SFE is observed with an increase in the concentration of microparticles on the Ti6Al4V scaffolds. However, for the samples prepared with 400 µl aliquot, values that did not correspond to the general trend (46.11±2.44 mN/m) were obtained. Note that the polar component of the surface free energy is the lowest for the control sample and scaffold prepared with 40 µl of microparticles. The authors of [63] noted the influence of the polar component of the surface free energy on fibroblast adhesion, which represents the interaction energy of the surface with water. It has been revealed that cellular adhesion is maximal when the fractional polarity, FP ($\gamma p/(\gamma p+\gamma d)$), where γp and γd are polar and dispersive components, respectively, is equal to 0.3. When an FP parameter was calculated using the Owens Wendt approach, the value of 0.21 for control samples, 0.13 for scaffolds prepared with 40 µl aliquots of DEX, and 0.40 and 0.67 for scaffolds prepared with 200 and 400 µl aliquot of DEX were obtained, respectively. Thus, the region with a fractional polarity of 0.21 might be expected to have the most appropriate fibroblast compatibility. Thus, it can be concluded that a low polar component (or a low fractional polarity) is a major parameter contributing to good fibroblast proliferation.

One can conclude that there is no clear relationship between the surface roughness parameters R_a, R_q, and R_t and the total apparent surface free energy. Nevertheless, generally, the polar interactions increase with decreasing surface roughness values, while the non-polar dispersion interactions do not depend on the topography and small changes in the chemistry of the surface caused by the deposition of particles. A similar behavior was found for Ti and its two different alloys reported elsewhere [64].

3.5 The study of the release of DEX

As noted above, the formation of PE shells is based on electrostatic interactions between oppositely charged functional groups of PEs. The conformation and charge of the functional groups

(ionization) of weak PEs depend on the acidity of the medium (pH). However, the charged groups of strong PEs mainly remain unchanged with changing pH. The combination of strong and weak PEs allows control over the permeability of the capsule shell. This property of microcapsules has found applications in the encapsulation and release of substances [22]. The combination of a weak cation (PAH) and a strong anion (PSS) makes it possible to create a permeable capsule shell [22, 65].

SEM results (Fig. 9) indicate that, after the "release" of DEX, the microparticles remain well fixed on the scaffold surface, even 7 days after the beginning of the experiments. This is explained by several factors, such as high surface roughness R_a (19 ± 1 μm), very high wettability (54.67 ± 4.17°), and strong electrostatic interactions between the positively charged Ti6Al4V scaffold surface and the negatively charged particle surfaces represented by the PSS anionite layer (-17.7 ± 1.58 mV).

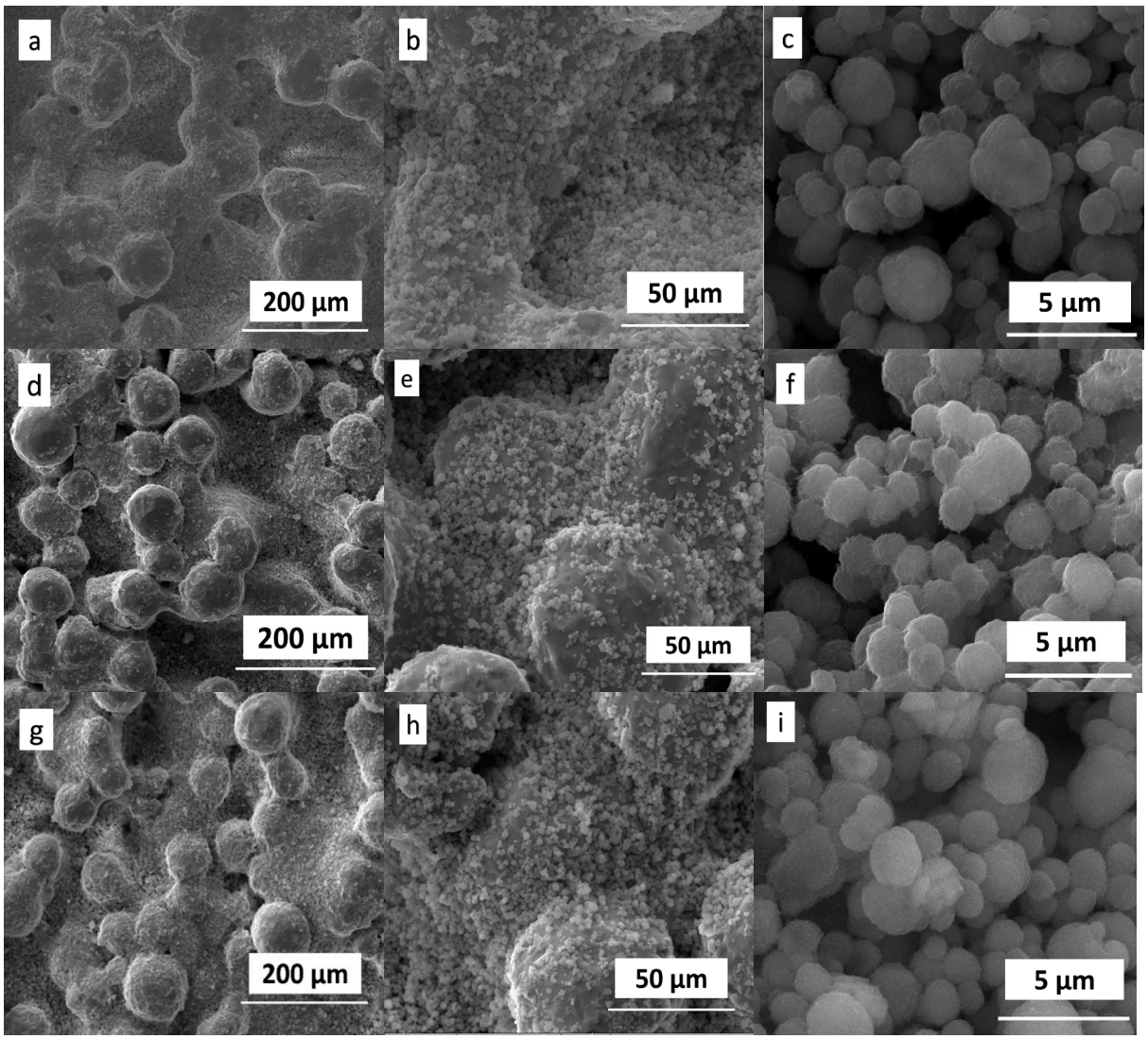

Figure 9 SEM images of the Ti6Al4V scaffolds functionalized with 400 µl aliquots of microparticles loaded with DEX 1 day (a-c), 3 days (d-f) and 7 days (g-h) after the microcapsules were dissolved.

Note that the PE microparticle shells became friable and highly permeable after the first day of the experiment (Fig. 9c), which was not observed in the SEM images of freshly prepared scaffolds (Fig. 2a), and this picture persisted for 3 (Fig. 9d-f) and 7 days (Fig. 9g-i). This is because PAH/PSS shells are able to gradually dissolve in an aqueous medium and can also respond to changes in their ionic composition. Due to the good adhesion of the microparticles on the scaffold surface and the high permeability of the PE shell, the calcium ions of the carbonate core will be able to actively participate in the osteogenesis process [66].

The rate of release of drugs from capsules depends significantly on the number of PAH/PSS bilayers that make up the capsule shell. The use of a small shell of three bilayers ensures the quick release and delivery of drugs to the tissues around the implanted scaffold, which will reduce or even prevent the inflammatory response of the recipient's body that occurs in the first hours of the postoperative period. The HPLC analysis data show that drug release from the scaffold surface occurs primarily on the first day (79.6 %). Furthermore, the drug concentration in the solution gradually decreased, and after 7 days, the drug content decreased by half, possibly due to hydrolysis processes (87.4 %).

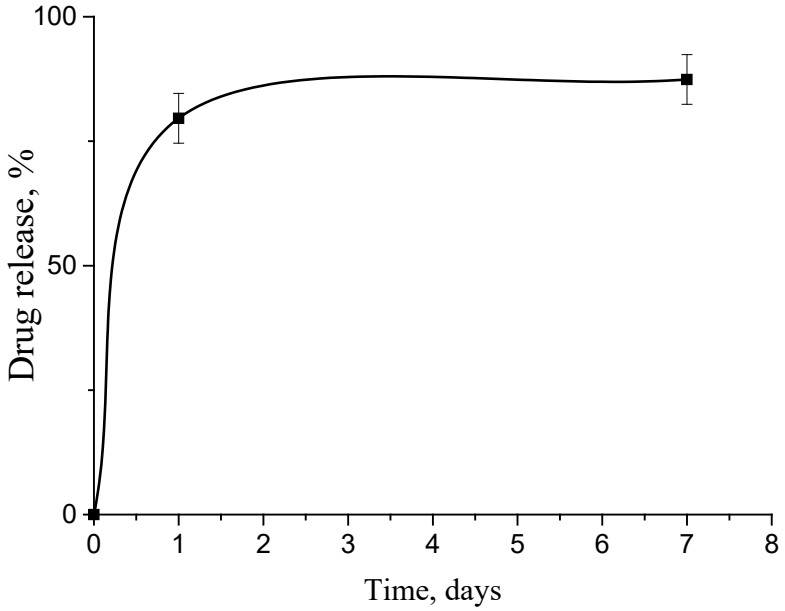

Figure 10 Release profile of DEX from the PEs coated $CaCO_3$ microparticles deposited on Ti6Al4V scaffolds.

Thus, microparticles manufactured using a specified procedure demonstrate a two-stage DEX release pattern, with an intense burst occurring in the first two days followed by sustained release until 7 days (Fig. 10). A similar release behavior was also observed by Qi et al. [67].

3.6 Cell morphology, adhesion and spreading

The surface topography plays an important role in cell adhesion and proliferation. Moreover, some reports have shown that cells can sense their microenvironment and respond by adjusting the organization of their cytoskeleton and the formation of focal adhesion points that bind the cell to the surface. Herein, the fibroblast adhesion behavior after 24 hours was investigated using scaffolds coated with microparticles prepared with different DEX concentrations and uncoated scaffolds as a control. The general shape and growth pattern of 3T3-L1 cells on the Ti6Al4V scaffolds modified by microparticles with different concentrations and those without DEX are demonstrated in Figure 11. The cells were found to be efficiently attached to the coated and un-coated scaffold surfaces.

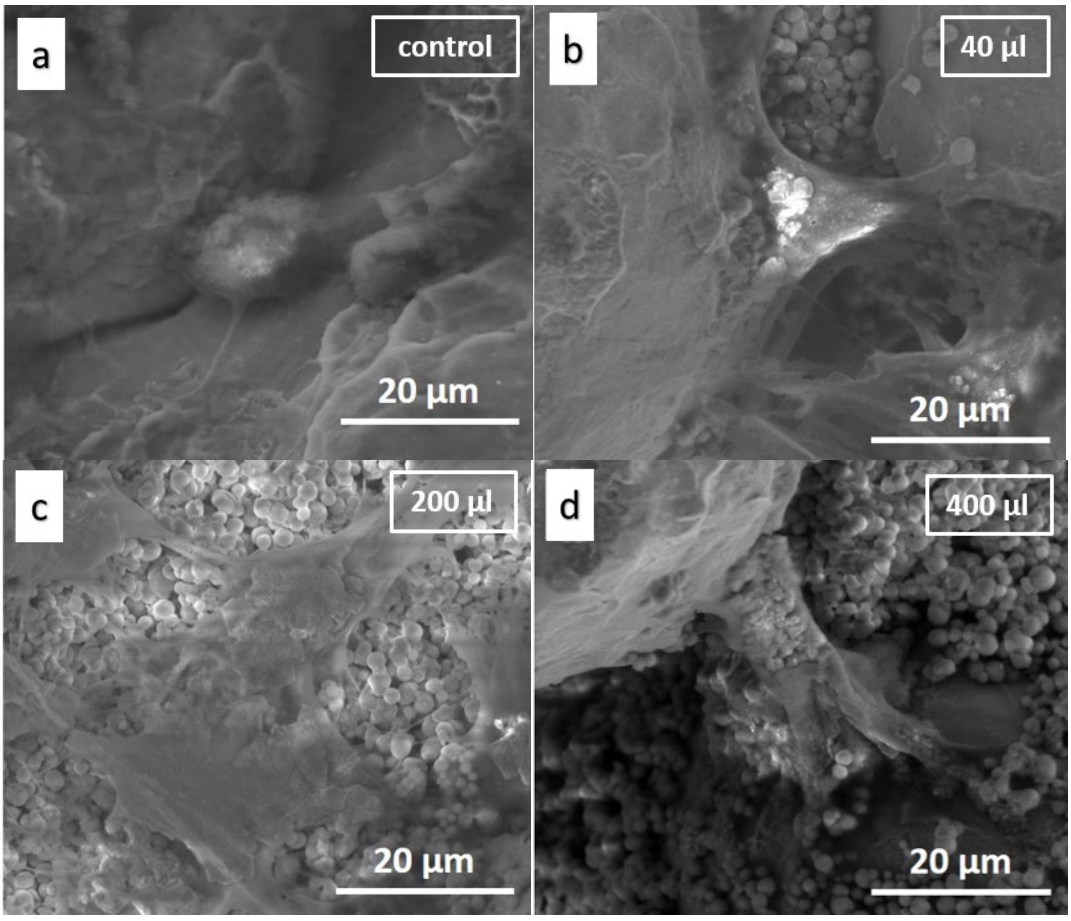

Figure 11 SEM images of fibroblast-attached Ti6Al4V scaffolds: unmodified surface (a) and scaffold functionalized via microspheres loaded with DEX and coated with PE bilayers at different concentrations (b-d).

As shown in micrographs (Fig. 11), cells grew and attached normally on scaffolds without surface modification. It should be noted that cells also grew normally on the surface of functionalized scaffolds; however, in the latter case they were spread over the larger surface area and revealed more elongated spindle-shaped form. According to Figure 11 (b-d) some microparticles are incorporated into the cells, so it can be assumed that the cells move along the surface and capture the particles. Normal cell proliferation is confirmed by the results of fluorescence microscopy (Fig. 12).

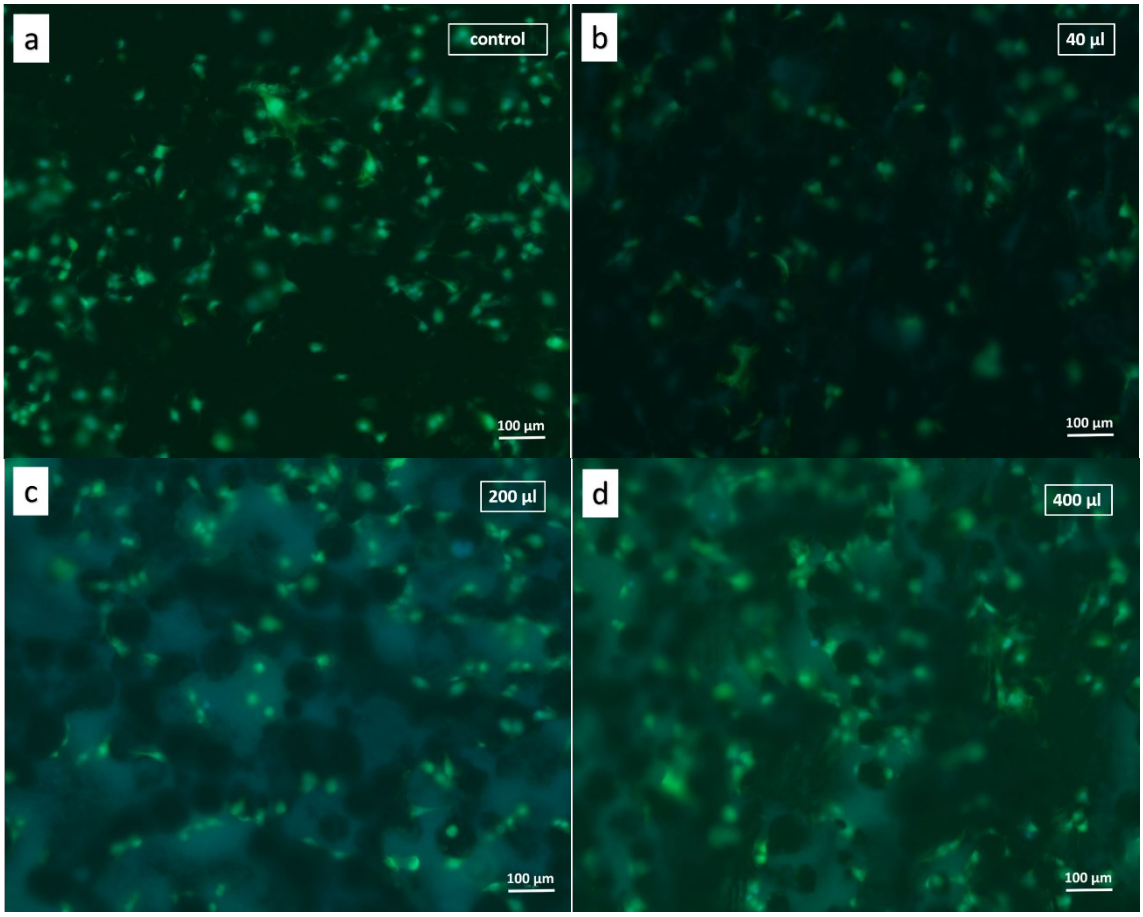

Figure 12 Fluorescent images of fibroblasts on Ti6Al4V scaffolds: unmodified surface (a) and functionalized scaffold via microspheres loaded with DEX and coated with PE bilayers with different concentrations (b-d).

As shown in Figure 12 (b,d), the cells can be dispersed in the surface valleys, and the cells are in contact with the rough scaffold, indicating that the Ti6Al4V scaffolds printed by the EBM® pro-

cess stimulate cell growth. The fact that topography of the scaffolds should be considered as a factor affecting the interactions between implants and tissues is also reported elsewhere [68].

Figure 13 presents the surface density (per mm^2) of the fibroblasts attached to the scaffolds calculated from fluorescence images. Calculations demonstrated that surface modification did not have a significant effect on fibroblasts after 24 hours compared with unmodified Ti6Al4V scaffolds. Thus, it can be concluded that DEX has no toxic effect.

It is widely accepted that cells react not only to the surface topography but also to the surface chemistry. However, there is a lack of data on how these factors act together in the generation of biological responses. This is mainly because it is quite difficult to separately change the surface roughness and composition. Some studies have been published on the relative influence of surface chemistry and surface topography on cell behavior. Hallab et al. [75] demonstrated that the surface free energy was more important than surface roughness for cellular adhesion and proliferation. The authors also applied gold–palladium coatings to metallic substrates with different roughnesses to demonstrate that short-term adhesion and proliferation were more dependent on surface composition, whereas long-term adhesion was more dependent on surface roughness [27, 44, 76–78].

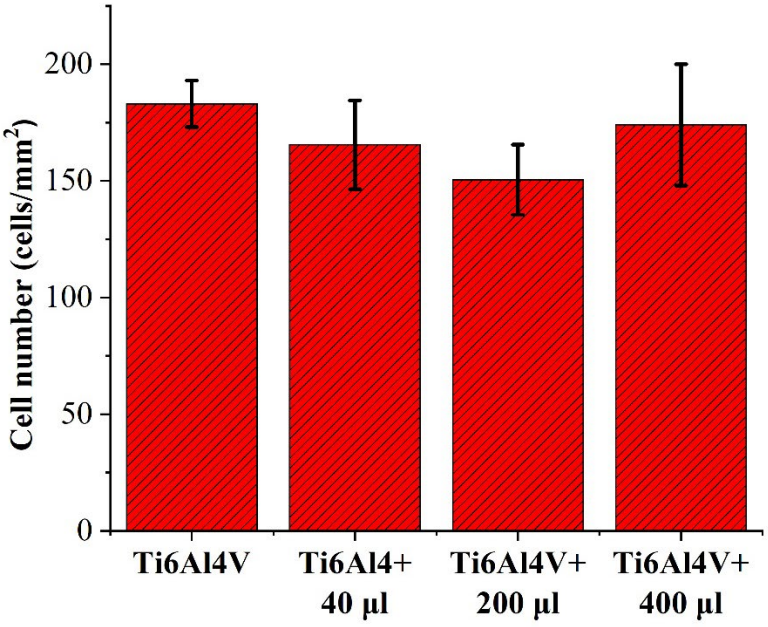

Figure 13 Cell density on the surface of the functionalized scaffold via microspheres loaded with DEX and coated with PE bilayers.

Based on the data calculated for the surface free energy, we can conclude that the data correlate with cell spreading. Our results indicate increasing relative cell growth with increasing surface free energy, which is similar to the results obtained elsewhere [69]. The relationship between cell spreading and surface free energy can be explained taking into account an interfacial free energy balance, predicting that cell spreading will be pronounced if the following condition is met such as:

$$\Delta F_{adh} \approx \gamma_{cs} - \gamma_{cl} - \gamma_{sl} < 0 \quad (1)$$

and cell spreading will be low if the following condition is met such as:

$$\Delta F_{adh} > 0 \quad (2)$$

where ΔF_{adh} is the interfacial free energy of adhesion, γ_{cs} is the cell-solid interfacial free energy, γ_{cl} is the cell-liquid interfacial free energy, and γ_{sl} is the solid-liquid interfacial free energy.

ΔF_{adh} can be calculated from the dispersion (γ^d) and polar (γ^p) components of the surface free energy of the solid γ_s, cell γ_c and the liquid γ_l (tissue culture medium) as described by Busscher et al. [70].

The effect of DEX on cell growth should be noted. It is possible that the decrease in cell growth activity is also associated with the inhibitory effect of this drug. It has been reported that glucocorticoids, including DEX, are important regulators of cell proliferation, and fibroblasts are one of the main targets of steroid action. Numerous studies aimed at investigating the effect of DEX have shown its inhibitory behavior on cell growth.

For example, the authors of the study [71] investigated the role of DEX in inhibiting inflammation and cartilage damage in a model of posttraumatic osteoarthritis. It was shown that DEX significantly decreases the concentration of basic fibroblast growth factor. The results obtained by Sun R. et al [72] have also shown that DEX can significantly inhibit human Tenon's capsule fi-

broblast growth in a cell culture model from days 1 to 7. The inhibitory effect was not observed when the cultures were switched after 24 hours to drug-free culture medium.

Liu L. et al [73] investigated the effect of DEX on resident naive cells. They used genome microarray and microRNA (miR) analyses to evaluate the global gene and miR expression of human corneal fibroblasts in response to treatment with DEX. The authors noted that some of the cell genes were downregulated more than threefold after DEX treatment. In addition, the expression of several miRs, including miR-100, was downregulated, whereas miR-16, miR-21, and miR-29C in fibroblasts were upregulated by DEX. All these results reflect the diverse and potentially tissue-specific nature of DEX action.

Different (stimulatory and inhibitory) DEX influences on cell growth were also reported for different cell types. It has also been suggested that the extent and direction of a given response to DEX can vary within the same cell type, depending on the metabolic state of the cells [74]. It has also been demonstrated that DEX inhibits the proliferation of mouse fibroblasts *in vitro* and rat fibroblasts in sparse cultures independent of cell density [75]. The main mechanism of glucocorticoid action is predominantly mediated through the glucocorticoid receptor (GR), which is expressed both *in vivo* and *in vitro*. However, the real mechanism of action is quite complex, since it was established that glucocorticoids act not through a single GR but through a diverse collection of receptor isoforms [76]. In the context of the obtained results, it should be considered that glucocorticoids in general and DEX in particular are systemic drugs. At the same time, the influence of glucocorticoids in certain conditions may not be well pronounced in cell cultures, or their impact will be weak. These hormones have the ability to suppress most inflammatory parameters, which makes glucocorticoids extremely effective anti-inflammatory drugs [77]. Therefore, the effects of glucocorticoids are largely manifested at the microorganism level, causing a cascade of reactions that cannot be simulated *in vitro*. First, the effects of glucocorticoids are realized in cooperation with the hypothalamic-pituitary system of the brain and the regulation of inflammatory processes by the humoral link of the immune system and effector immunocompe-

tent cells. The impact and regulation of immune processes is an important challenge that must be considered when creating biomaterials [78]. The complex, multicomponent signals of the endocrine system acting through cell receptors or neuroendocrine pathways can influence regeneration by modulating the immune response to injury or by enhancing or suppressing proliferation and differentiation pathways in target tissues [79]. Maladjustment of regulation leads to numerous undesirable effects of glucocorticoids [80]. It is also important to note that at present, the adaptive and regulatory role of the cellular microenvironment is undoubted [81]. As applied to a macroorganism, this can have an important effect on the biocompatibility of artificial materials and the adaptation of connective tissue to them. In this context, the role of DEX may be key in this process, allowing for a reduction in local inflammation and having a positive effect on tissue regeneration *in vivo*.

The spatial and mechanical properties of microparticles can also affect cell behavior. For example, Evans found [82] that hydroxyapatite particles with a mean size of approximately 250 μm had no effect on cell growth. Particles with a mean size of 6-7 μm caused a reduction in the cell numbers to approximately one-third, and particles with a mean size of approximately 3.5 μm caused a reduction in cell numbers to approximately one-sixth at four days. This finding extends the earlier observations of Rae [83] that particulate metals may damage macrophages and fibroblasts in culture and may be hemolytic to red blood cells. Another experiment was carried out with three fractions of biphasic calcium phosphate microparticles, <20, 40–80 and 80–200 μm, after crushing [84]. The number of macrophages was relatively higher for the smallest than for the intermediate and largest fractions ($p< 0.0001$). The relative percentage of giant cells was higher for the intermediate and largest sizes of particles than for the smallest. Therefore, biphasic calcium phosphate microparticles with sizes <20 μm initiated an inflammatory response that might play an important role in osteogenesis. Lu et al [85] studied the influence of microparticle concentrations using hydroxyapatite, β-tricalcium phosphate and a 40% β-tricalcium phosphate/60% hydroxyapatite mixture *in vitro*. A decrease in cell viability was observed with the

increase in particle concentration. At 10 000 particles per cell, there were no viable cells, and their proliferation was completely inhibited.

Analysis of the literature has shown that the polymer layers that cover the particles also affect cell proliferation. At titanium surfaces covered with PAH/PSS composite films, cells showed fast proliferation and a large spreading area and formed numerous and well organized adhesion points. This indicated the great affinity of fibroblasts for the LbL-assembled nanocomposites [86].

The authors of the study [87] noted that for PSS/PAH films, PAH-terminated films result in better cell proliferation than PSS-terminated films. On the other hand, the PSS-terminated films, which were previously found to be biocompatible with PDL fibroblast cells [88], do not cause enhanced proliferation.

There are different opinions on the effect of surface roughness on cell behavior. According to the results reported elsewhere on the effects of surface roughness, fibroblasts reveal a more uniform distribution on compact scaffolds than on porous scaffolds [68]. Kunzler et al. [89] showed that fibroblasts exhibited a higher initial attachment on a rougher sample surface, proliferation slowed down rapidly after 4 days, and the number of cells on the smooth surface exceeded that on the rougher sample surface after 8 days. Thus, in addition to the surface roughness, there are another factors affecting proliferation of cells on the surface such as chemistry, wetting behavior etc.

Conclusion

We functionalized additively manufactured Ti6Al4V scaffolds using $CaCO_3$ microparticles loaded with DEX at three different concentrations and coated with the PE bilayers PAH/PSS. With the proposed method of synthesis, the microparticles are spherical with a rather narrow size distribution between 0.5 and 2.5 μm. Such a synthesis also allows for the increased loading of microparticles with the drug. As confirmed by UV spectroscopy, the DEX concentration in the mi-

croparticles reached 40 %. Drug loading can be further increased by increasing the number of polymer layers. The DEX-loaded particles showed a two-stage drug release profile: burst release at early hours followed by a sustained release period that lasted up to 7 days. IR analysis revealed the presence of bonds typical for DEX, $CaCO_3$ and the polymers involved in the synthesis of the microparticles. After deposition, the microparticles show a well-defined distribution on the surface after deposition. With increasing microparticle surface density, the average roughness decreases. In addition, functionalization of the titanium alloy scaffolds promoted the change from hydrophobic surface to hydrophilic one with a water contact angle below 5°. A higher number of cells on the Ti6Al4V scaffolds without modification reveal a spherical shape, while cells seeded on the functionalized scaffolds were better spread and reveal spindle-shaped cell morphology. In further, *in vitro* results revealed that scaffolds modified with $CaCO_3$ microparticles loaded with DEX have no toxic effect and can be used for further *in vivo* tests as anti-inflammatory drugs.

Acknowledgments:

This research was funded by the Ministry of Science and Higher Education of the Russian Federation (State Project “Science” №WSWW-2020-0011) and Tomsk Polytechnic University within the framework of a Tomsk Polytechnic University Competitiveness Enhancement Program grant. Mrs. Chudinova thanks the personal financial support from the G-RISC program funded by the German Federal Foreign Office via the German Academic Exchange Service (DAAD).

Declarations

Conflict of interest: The authors declare that they have no conflict of interest.

References

[1] Jarosz M, Pawlik A, Szuwarzynski M, Jaskula M, Sulka GD (2016) Nanoporous anodic titanium dioxide layers as potential drug delivery systems: Drug release kinetics and mechanism. Colloids Surf B 143: 447-454. doi:10.1016/j.colsurfb.2016.03.073

[2] Aninwene GE, II CY, Webster TJ (2008) Enhanced osteoblast adhesion to drug-coated anodized nanotubular titanium surfaces. Int J Nanomed 3(2): 257. doi:10.2147/IJN.S2552

[3] Bedouin Y, Gordin DM, Pellen-Mussiet al (2019) Enhancement of the biocompatibility by surface nitriding of a low-modulus titanium alloy for dental implant applications. J Biomed Mater Res Part B 107(5): 1483-1490. doi:10.1002/jbm.b.34240

[4] Majumdar T, Eisenstein N, Frith JE, Cox SC, Birbilis N (2018) Additive manufacturing of titanium alloys for orthopedic applications: a materials science viewpoint. Adv Eng Mater 20(9): 1800172. doi:10.1002/adem.201800172

[5] Sirivisoot S, Pareta R, Webster TJ (2011) Electrically controlled drug release from nanostructured polypyrrole coated on titanium. Nanotechnology 22(8): 085101.doi:10.1088/0957-4484/22/8/085101

[6] McLaughlin F, Mackintosh J, Hayes et al (2002) Glucocorticoid-induced osteopenia in the mouse as assessed by histomorphometry, microcomputed tomography, and biochemical markers. Bone 30(6): 924-930.doi:10.1016/S8756-3282(02)00737-8

[7] Yoon JJ, Kim JH, Park TG(2003) Dexamethasone-releasing biodegradable polymer scaffolds fabricated by a gas-foaming/salt-leaching method. Biomaterials 24(13): 2323-2329. doi:10.1016/S0142-9612(03)00024-3

[8] Zhang L, Yan J, Yin Z et al (2014) Electrospun vancomycin-loaded coating on titanium implants for the prevention of implant-associated infections. Int J Nanomed 9: 3027. doi:10.2147/IJN.S63991

[9] Ghiasi B, Sefidbakht Y, Mozaffari-Jovin et al (2020) Hydroxyapatite as a biomaterial–a gift that keeps on giving. Drug Dev Ind Pharm 46(7): 1035-1062. doi:10.1080/03639045.2020.1776321

[10] Bahrom H, Goncharenko AA, Fatkhutdinova et al (2019) Controllable Synthesis of Calcium Carbonate with Different Geometry: Comprehensive Analysis of Particle Formation, Cellular Uptake, and Biocompatibility. ACS Sustainable Chem Eng 7(23): 19142-19156. doi:10.1021/acssuschemeng.9b05128

[11] Maleki S, Barzegar-Jalali M, Zarrintan MH, Adibkia K, Lotfipour F (2015) Calcium carbonate nanoparticles; potential applications in bone and tooth disorders. Pharm Sci 20(4):175-182.

[12]Surmeneva MA, Chudinov EA, Chernozem et al (2020) Development of a bone substitute material based on additive manufactured Ti6Al4V alloys modified with bioceramic calcium carbonate coating: Characterization and antimicrobial properties. Ceram Int 46(16): 25661-25670.doi:10.1016/j.ceramint.2020.07.041

[13] Koptyug A, Rännar LE, Bäckström M, Fager Franzen S, Derand P (2013) Additive manufacturing technology applications targeting practical surgery. Int J Life Sci 3(1): 15-24. doi:10.5963/LSMR0301003

[14] Raj V, Prabha G (2016) Synthesis, characterization and in vitro drug release of cisplatin loaded Cassava starch acetate–PEG/gelatin nanocomposites. J Assoc Arab Univ 21: 10-16.doi:10.1016/j.jaubas.2015.08.001

[15] Timin AS, Muslimov AR, Zyuzin et al (2018) Multifunctional scaffolds with improved antimicrobial properties and osteogenicity based on piezoelectric electrospun fibers decorated with bioactive composite microcapsules. ACS Appl Mater Interfaces 10(41): 34849-34868.doi:10.1021/acsami.8b09810

[16] Svenskaya YI, Fattah H, Inozemtseva OA, Ivanova AG, Shtykov SN, Gorin DA, Parakhonskiy BV(2018) Key parameters for size-and shape-controlled synthesis of vaterite particles. Cryst Growth Des 18(1): 331-337. doi:10.1021/acs.cgd.7b01328

[17] Trushina DB, Bukreeva TV, Antipina MN (2016) Size-controlled synthesis of vaterite calcium carbonate by the mixing method: aiming for nanosized particles. Cryst Growth Des 16(3): 1311-1319.doi:10.1021/acs.cgd.5b01422

[18] Hanafy NAN, De Giorgi ML, Nobile C, Rinaldi R, Leporatti S (2015) Control of colloidal CaCO3 suspension by using biodegradable polymers during fabrication. Beni-Suef Univ J Appl 4(1): 60-70.doi:10.1016/j.bjbas.2015.02.009

[19] Jayant RD, McShane MJ, Srivastava R (2009) Polyelectrolyte-coated alginate microspheres as drug delivery carriers for dexamethasone release. Drug Deliv 16(6): 331-340. doi:10.1080/10717540903031126

[20] Kurapati R, Raichur AM (2013) Composite cyclodextrin–calcium carbonate porous microparticles and modified multilayer capsules: novel carriers for encapsulation of hydrophobic drugs. J Mater Chem B 1 (25): 3175-3184. doi:10.1039/C3TB20192A

[21] Radhakrishnan K, Vincent A, Joseph RR, Moreno M, Dickescheid A, Agrawal R, Venkatraman S (2019) Hollow Microcapsules as Periocular Drug Depot for Sustained Release of Anti-VEGF Protein. Pharmaceutics 11(7): 330.doi.org/10.3390/pharmaceutics11070330

[22] Sukhorukov GB, Volodkin DV, Günther et al (2004) Porous calcium carbonate microparticles as templates for encapsulation of bioactive compounds. J Mater Chem 14: 2073-2081.doi:10.1039/B402617A

[23] Seijo B, Fattal E, Roblot-Treupel L, Couvreur P (1990) Design of nanoparticles of less than 50 nm diameter: preparation, characterization and drug loading. International journal of pharmaceutics 62(1): 1-7. doi:10.1016/0378-5173(90)90024-X

[24] Song CX, Labhasetwar V, Murphy H, Qu X, Humphrey WR, Shebuski RJ, Levy RJ (1997) Formulation and characterization of biodegradable nanoparticles for intravascular local drug delivery. Journal of Controlled Release 43(2-3): 197-212.doi:10.1016/S0168-3659(96)01484-8

[25] Fessi H, Puisieux F, Devissaguet JP, Ammoury N,Benita S (1989) Nanocapsule formation by interfacial polymer deposition following solvent displacement. Int J Pharm 55(1): R1-R4.doi:10.1016/0378-5173(89)90281-0

[26] Solid-state solubility influences encapsulation and release of hydrophobic drugs from PLGA/PLA nanoparticles. J Pharm Sci 93(7): 1804-1814.doi:10.1002/jps.20094

[27] Mandapalli PK, Labala S, Vanamala D, Koranglekar MP, Sakimalla LA, Venuganti VV. K (2014) Influence of charge on encapsulation and release behavior of small molecules in self-assembled layer-by-layer microcapsules. Drug Deliv 21(8): 605-614.doi:10.3109/10717544.2013.867381

[28] Wang Z, Ma Y, Wei J et al (2017) Effects of sintering temperature on surface morphology/microstructure, in vitro degradability, mineralization and osteoblast response to magnesium phosphate as biomedical material. Sci Rep 7(1): 1-11.doi:10.1038/s41598-017-00905-2

[29] Kamyar A, Khakbiz M, Zamanian A, Yasaei M, Yarmand B (2019) Synthesis of a novel dexamethasone intercalated layered double hydroxide nanohybrids and their deposition on anodized titanium nanotubes for drug delivery purposes. J Solid State Chem 271: 144-153.doi:10.1016/j.jssc.2018.12.043

[30] Shivkumara C, Singh P, Gupta A, Hegde MS (2006) Synthesis of vaterite CaCO3 by direct precipitation using glycine and L-alanine as directing agents, Mater Res Bull 41(8): 1455-1460.doi:10.1016/j.materresbull.2006.01.026

[31] Beniash E, Aizenberg J, Addadi L, Weiner S (1997) Amorphous calcium carbonate transforms into calcite during sea urchin larval spicule growth. Proceedings of the Royal Society of London. Series B: Biological Sciences 264(1380): 461-465.doi:10.1098/rspb.1997.0066

[32] Chakkarapani P, Subbiah L, Palanisamy S, Bibiana A, Ahrentorp F, Jonasson C, Johansson C (2015) Encapsulation of methotrexate loaded magnetic microcapsules for magnetic drug targeting and controlled drug release. J Magn Magn Mater 380: 285-294.doi:10.1016/j.jmmm.2014.11.006

[33] Wang Y, Moo YX, Chen C, Gunawan P, Xu R (2010) Fast precipitation of uniform CaCO3 nanospheres and their transformation to hollow hydroxyapatite nanospheres. J Colloid Interface Sci 352(2): 393-400. doi:10.1016/j.jcis.2010.08.060

[34] Awada H, Montplaisir D, Daneault C (2012) Growth of polyelectrolyte on lignocellulosic fibres: Study by zeta potential, FTIR, and XPS. BioResources 7(2): 2090-2104. doi:10.1149/2.0801504jes

[35] Lee J, Choi W (2015) Surface Modification of Over-Lithiated Layered Oxides with PE-DOT:PSS Conducting Polymer in Lithium-Ion Batteries. J Electrochem Soc 162:A743-A748.

[36] Estrela-Lopis I, Iturri Ramos JJ, Donath E, Moya SE (2010) Spectroscopic studies on the competitive interaction between polystyrene sodium sulfonate with polycations and the N-tetradecyl trimethyl ammonium bromide surfactant. J Phys Chem B 114(1): 84-9. doi:10.1021/jp908608u

[37] Li L, Ma R, Iyi N, Ebina Y, Takada K, Sasaki T (2006) Hollow nanoshell of layered double hydroxide. Chem Commun (29): 3125-3127. doi:10.1039/B605889B

[38] de Damborenea JJ, Larosa MA, Arenas MA, Hernandez-Lopez JM, Jardini AL, Ierardi MC F, Conde A (2015) Functionalization of Ti6Al4V scaffolds produced by direct metal laser for biomedical applications. Mater Des 83: 6-13. doi: 10.1016/j.matdes.2015.05.078

[39] Li Y, Yang W, Li X et al (2015) Improving osteointegration and osteogenesis of three-dimensional porous Ti6Al4V scaffolds by polydopamine-assisted biomimetic hydroxyapatite coating. ACS Appl Mater Interfaces 7(10): 5715-5724. doi: 10.1021/acsami.5b00331

[40] Douglas TE, Hempel U, Żydek J, Vladescu A, Pietryga K, Kaeswurm JA, Buchweitz M, Surmenev RA, Surmeneva MA, Cotrut C, Koptyug AV, Pamuład E (2018) Pectin coatings on titanium alloy scaffolds produced by additive manufacturing: Promotion of human bone marrow stromal cell proliferation. Mater lett (227): 225-228.

[41] Shuai C, He C, Qian G, Min A, Deng Y, Yang W, Zang X. (2021) Mechanically driving supersaturated Fe–Mg solid solution for bone implant: preparation, solubility and degradation. Compos B Eng (207): 108564. doi.org/10.1016/j.compositesb.2020.108564

[42] Yang Y, Cheng Y, Peng S, Xu L, He C, Qi F, Zhao M, Shuai C. (2021). Microstructure evolution and texture tailoring of reduced graphene oxide reinforced Zn scaffold. Bioact Mater 6(5): 1230-1241. doi.org/10.1016/j.bioactmat.2020.10.017

[43] Karpov TE, Peltek OO, Muslimov et al (2019) Development of Optimized Strategies for Growth Factor Incorporation onto Electrospun Fibrous Scaffolds To Promote Prolonged Release. ACS Appl Mater Interfaces 12(5): 5578-5592. doi: 10.1021/acsami.9b20697

[44] Li Q, Rudolph V, Weigl B, Earl A (2004) Interparticle van der Waals force in powder flowability and compactibility. Int J Pharm 280(1-2): 77-93. doi: 10.1016/j.ijpharm.2004.05.001

[45] Nelea V, Kaartinen MT (2010) Periodic beaded-filament assembly of fibronectin on negatively charged surface. J Struct Biol 170(1): 50-59 doi: 10.1016/j.jsb.2010.01.009

[46] Gongadze E, Kabaso D, Bauer S, Slivnik T, Schmuki P, Van Rienen U, Iglič A (2011) Adhesion of osteoblasts to a nanorough titanium implant surface. Int J Nanomed 6: 1801. doi: 10.2147/IJN.S21755

[47] Rapuano BE, MacDonald DE (2011) Surface oxide net charge of a titanium alloy: modulation of fibronectin-activated attachment and spreading of osteogenic cells. Colloids Surf 82(1): 95-103. doi: 10.1016/j.colsurfb.2010.08.023

[48] Roessler S, Zimmermann R, Scharnweber D, Werner C, Worch H (2002) Characterization of oxide layers on Ti6Al4V and titanium by streaming potential and streaming current measurements. Colloids Surf B 26(4): 387-395. doi: 10.1016/S0927-7765(02)00025-5

[49] Jonasova L, Müller FA, Helebrant A, Strnad J, Greil P (2004) Biomimetic apatite formation on chemically treated titanium. Biomaterials 25(7-8): 1187-1194. doi: 10.1016/j.biomaterials.2003.08.009

[50] Cordero ZC, Meyer III HM, Nandwana P, Dehoff RR (2017) Powder bed charging during electron-beam additive manufacturing. Acta Mater 124: 437-445. doi: 10.1016/j.actamat.2016.11.012

[51] Tong W, Dong W, Gao C, Möhwald H (2005) Charge-controlled permeability of polyelectrolyte microcapsules. J Phys Chem 109(27): 13159-13165. doi: 10.1021/jp0511092

[52] Kiel M, Klötzer M, Mitzscherling S, Bargheer M (2012) Measuring the range of plasmonic interaction. Langmuir 28(10): 4800-4804. doi: 10.1021/la204577m

[53] You S, Wan MP (2013) Mathematical models for the van der Waals force and capillary force between a rough particle and surface. Langmuir 29(29): 9104-9117. doi: 10.1021/la401516m

[54] Yang L, Hu J, Bai K (2016) Capillary and van der Waals force between microparticles with different sizes in humid air. J Adhes Sci Technol 30(5), 566-578, doi: 10.1080/01694243.2015.1111834

[55] Zhao G, Raines AL, Wieland M, Schwartz Z, Boyan BD (2007) Requirement for both micron-and submicron scale structure for synergistic responses of osteoblasts to substrate surface energy and topography. Biomaterials 28(18): 2821-2829. doi: 10.1016/j.biomaterials.2007.02.024

[56] Kolasinska M, Warszynski P (2005) The effect of support material and conditioning on wettability of PAH/PSS multilayer films. Bioelectrochemistry 66(1-2): 65-70, doi: 10.1016/j.bioelechem.2004.03.009

[57] Adamczyk Z, Zembala M, Kolasinska M, Warszynski P (2007) Characterization of polyelectrolyte multilayers on mica and oxidized titanium by streaming potential and wetting angle measurements. Colloids Surf A 302(1-3): 455-460. doi: 10.1016/j.colsurfa.2007.03.013

[58] Kawamura G, Ema T, Sakamoto H, Wei X, Muto H, Matsuda A (2014) Spontaneous changes in contact angle of water and oil on novel flip–flop-type hydrophobic multilayer coatings. Appl Surf Sci 298: 142-146. doi: 10.1016/j.apsusc.2014.01.143

[59] Elzbieciak M, Kolasinska M, Warszynski P (2008) Characteristics of polyelectrolyte multilayers: The effect of polyion charge on thickness and wetting properties. Colloids Surf A 321(1-3): 258-261. doi: 10.1016/j.colsurfa.2008.01.036

[60] Wong JE, Rehfeldt F, Hänni P, Tanaka M, Klitzing RV (2004) Swelling behavior of polyelectrolyte multilayers in saturated water vapor. Macromolecules 37(19): 7285-7289, doi: 10.1021/ma0351930

[61] Sajid HU, Kiran R (2018) Kiran, Influence of corrosion and surface roughness on wettability of ASTM A36 steels. J Constr Steel Res 144: 310-326. doi: 10.1016/j.jcsr.2018.01.023

[62] Chen W, McCarthy TJ (1997) Layer-by-layer deposition: a tool for polymer surface modification. Macromolecules 30(1): 78-86. doi: 10.1021/ma961096d

[63] Ponsonnet L, Reybier K, Jaffrezic N, Comte V, Lagneau C, Lissac M, Martelet C (2003) Relationship between surface properties (roughness, wettability) of titanium and titanium alloys and cell behaviour. Mat Sci Eng 23(4): 551-560. doi: 10.1016/S0928-4931(03)00033-X

[64] Yan Y, Chibowski E, Szczes A (2017) Surface properties of Ti-6Al-4V alloy part I: Surface roughness and apparent surface free energy. Mater Sci Eng: C 70: 207-215. doi: 10.1016/j.msec.2016.08.080

[65] Volodkin DV, Petrov AI, Prevot M, Sukhorukov GB (2004) Matrix polyelectrolyte microcapsules: new system for macromolecule encapsulation. Langmuir 20(8): 3398-3406. doi: 10.1021/la036177z

[66] Wang Q, Zhong S, Ouyang J, Jiang L, Zhang Z, Xie, Y, Luo S (1998) Osteogenesis of electrically stimulated bone cells mediated in part by calcium ions. Clin Orthop Relat (348): 259-268.

[67] Qi H, Chen Q, Ren H, Wu X, Liu X, Lu T (2018) Electrophoretic deposition of dexamethasone-loaded gelatin nanospheres/chitosan coating and its dual function in anti-inflammation and osteogenesis. Colloids Surf B 69: 249-256. doi: 10.1016/j.colsurfb.2018.05.029

[68] Liu J, Jin F, Zheng ML, Wang S, Fan SQ, Li P, Duan XM (2019) Cell Behavior on 3D Ti-6Al-4 V Scaffolds with Different Porosities. ACS Appl Bio Mater 2(2): 697-703. doi: 10.1021/acsabm.8b00550

[69] Schakenraad JM, Busscher HJ, Wildevuur CR, Arends J (1986) The influence of substratum surface free energy on growth and spreading of human fibroblasts in the presence and absence of serum proteins. J Biomed Mater Res 20(6): 773-784. doi: 10.1002/jbm.820200609

[70] Busscher HJ, Weerkamp AH, van der Mei HC, Van Pelt AW, de Jong HP, Arends J (1984) Measurement of the surface free energy of bacterial cell surfaces and its relevance for adhesion. Appl Environ Microbiol 48(5): 980-983.

[71] Huebner KD, Shrive NG, Frank CB (2014) Dexamethasone inhibits inflammation and cartilage damage in a new model of post-traumatic osteoarthritis. J Orthop Res 32(4): 566-572. doi: 10.1002/jor.22568

[72] Sun R, Gimbel HV, Liu S, Guo D, Hollenberg M D (1999) Effect of diclofenac sodium and dexamethasone on cultured human Tenon's capsule fibroblasts. Ophthalmic Surg Lasers Imaging Retina 30: 382-388. doi: 10.3928/1542-8877-19990501-19

[73] Liu L, Walker EA, Kissane S, Khan I, Murray PI, Rauz S, Wallace GR (2011) Gene expression and miR profiles of human corneal fibroblasts in response to dexamethasone. Invest Ophthalmol Visual Sci 52(10): 7282-7288. doi: 10.1167/iovs.11-7463

[74] TL Chen, CM Cone, D Feldman (1983) Glucocorticoid modulation of cell proliferation in cultured osteoblast-like bone cells: differences between rat and mouse. Endocrinology 112(5): 1739-1745.

[75] Pratt WB, Aronow L (1966) The effect of glucocorticoids on protein and nucleic acid synthesis in mouse fibroblasts growing in vitro. J Biol Chem 241(22): 5244-5250. doi: 10.1016/S0021-9258(18)96424-0

[76] Ramamoorthy S, Cidlowski JA (2016) Corticosteroids: mechanisms of action in health and disease. Rheum Dis Clin 42(1): 15-31. doi: 10.1016/j.rdc.2015.08.002

[77] Newton R (2000) Molecular mechanisms of glucocorticoid action: what is important?. Thorax 55(7): 603-613. doi: 10.1136/thorax.55.7.603

[78] Smith TD, Nagalla RR, Chen EY, Liu WF (2017) Harnessing macrophage plasticity for tissue regeneration. Adv Drug Delivery Rev 114: 193-205. doi: 10.1016/j.addr.2017.04.012

[79] Easterling MR, Engbrecht KM, Crespi EJ (2019) Endocrine regulation of regeneration: Linking global signals to local processes. Gen Comp Endocrinol 283: 113220. doi:10.1016/j.ygcen.2019.113220

[80] Schäcke H, Döcke WD, Asadullah K (2002) Mechanisms involved in the side effects of glucocorticoids. Pharmacol Ther 96(1): 23-43. doi: 10.1016/S0163-7258(02)00297-8

[81] Wang Y, Chen X, Cao W, Shi Y (2014) Plasticity of mesenchymal stem cells in immunomodulation: pathological and therapeutic implications. Nat Immunol 15(11): 1009.

[82] Evans EJ, Clarke-Smith EMH (1991) Studies on the mechanism of cell damage by finely ground hydroxyapatite particles in vitro. Clin Mater 7(3): 241-245. doi: 10.1016/0267-6605(91)90065-N

[83] Rae T (1975) A study on the effects of particulate metals of orthopaedic interest on murine macrophages in vitro. British volume J Bone Surg 57(4): 444-450. doi: 10.1302/0301-620X.57B4.444

[84] Fellah BH, Josselin N, Chappard D, Weiss P, Layrolle P (2007) Inflammatory reaction in rats muscle after implantation of biphasic calcium phosphate micro particles. J Mater Sci Mater Med 18(2): 287-294. doi: 10.1007/s10856-006-0691-8

[85] Lu J, Blary MC, Vavasseur S, Descamps M, Anselme K, Hardouin P (2004 Relationship between bioceramics sintering and micro-particles-induced cellular damages. J Mater Sci Mater Med 15(4): 361-365. doi: 10.1023/B:JMSM.0000021102.68509.65

[86]Qi W, Xue Z, Yuan W, Wang H (2014) Layer-by-layer assembled graphene oxide composite films for enhanced mechanical properties and fibroblast cell affinity. J Mater Chem B 2(3): 325-331. doi:10.1039/C3TB21387K

[87] Mhamdi L, Picart C, Lagneau C, Othmane A, Grosgogeat B, Jaffrezic-Renault N, Ponsonnet L (2006) Study of the polyelectrolyte multilayer thin films' properties and correlation with the behavior of the human gingival fibroblasts. Mater Sci Eng C 26(2-3): 273-281 doi: 10.1016/j.msec.2005.10.049

[88] Tryoen-Toth P, Vautier D, Haikel Y, Voegel JC, Schaaf P, Chluba J, Ogier J (2002) Viability, adhesion, and bone phenotype of osteoblast-like cells on polyelectrolyte multilayer films. J Biomed Mater Res 60(4): 657-667. doi: 10.1002/jbm.10110.

[89] Kunzler TP, Drobek T, Schuler M, Spencer ND (2007) Systematic study of osteoblast and fibroblast response to roughness by means of surface-morphology gradients. Biomaterials 28(13): 2175-2182. doi: 10.1016/j.biomaterials.2007.01.019